

Published in final edited form as:

J Med Chem. 2015 January 22; 58(2): 665–681. doi:10.1021/jm501165d.

Probing the Carboxyester Side Chain in Controlled Deactivation (–)-⁸-Tetrahydrocannabinols

Spyros P. Nikas^{†, #}, Rishi Sharma^{†, †, #}, Carol A. Paronis[†], Shashank Kulkarni[†], Ganesh A. Thakur[†], Dow Hurst[‡], JodiAnne T. Wood[†], Roger S. Gifford[†], Girija Rajarshi[†], Yingpeng Liu[†], Jimit Girish Raghav[†], Jason Jianxin Guo[†], Torbjörn U.C. Järbe[†], Patricia H. Reggio[‡], Jack Bergman[§], and Alexandros Makriyannis^{†, ||, *}

[†]Center for Drug Discovery and Departments of Chemistry and Chemical Biology and Pharmaceutical Sciences, Northeastern University, Boston, Massachusetts 02115, United States

[‡]Center for Drug Discovery, University of North Carolina at Greensboro, Greensboro, North Carolina 27402, United States

[§]McLean Hospital, Harvard Medical School, Belmont, Massachusetts 02478, United States

^{||}King Abdulaziz University, Jeddah 22254, Saudi Arabia

Abstract



We recently reported on a controlled deactivation/detoxification approach for obtaining cannabinoids with improved druggability. Our design incorporates a metabolically labile ester group at strategic positions within the THC structure. We have now synthesized a series of (–)-⁸-THC analogues encompassing a carboxyester group within the 3-alkyl chain in an effort to explore this novel cannabinergic chemo-type for CB receptor binding affinity, in vitro and in vivo potency and efficacy, as well as controlled deactivation by plasma esterases. We have also probed the chain's polar characteristics with regard to fast onset and short duration of action. Our lead

© 2014 American Chemical Society

*Corresponding Author: Phone: +1-617-373-4200. Fax: +1-617-373-7493. a. makriyannis@neu.edu. Address: Center for Drug Discovery and Departments of Chemistry and Chemical Biology and Pharmaceutical Sciences, Northeastern University, 360 Huntington Avenue, 116 Mugar Hall, Boston, MA, 02115, United States.

[†]Present Address

(For R.S.) Rishi Sharma Microconstants Inc., 10191 Caminito Volar, San Diego California 92126, United States; E-mail, sharmarishi2004@yahoo.co.in.

#Author Contributions

S.P.N. and R.S. contributed equally to this work.

The authors declare no competing financial interest.

Supporting Information

Elemental analysis results for compounds **6b**, **7c**, **9b**, **9d**, **10a**, and **16**, tables for molecular modeling, hypothermic effects of approximately equivalent doses of **10a**, **2b**, and ⁸-THC-DMH at different times after injection, and tail flick latencies in a hot water bath after administration of **10a**. This material is available free of charge via the Internet at <http://pubs.acs.org>.

molecule, namely 2-[(6a*R*,10a*R*)-6a,7,10,10a-tetrahydro-1-hydroxy-6,6,9-trimethyl-6*H*-dibenzo[*b,d*]pyran-3-yl]-2-methyl-propanoic acid 3-cyano-propyl ester (AM7438), showed picomolar affinity for CB receptors and is deactivated by plasma esterases while the respective acid metabolite is inactive. In further *in vitro* and *in vivo* experiments, the compound was found to be a remarkably potent and efficacious CB1 receptor agonist with relatively fast onset/offset of action.

INTRODUCTION

(-)-⁹-Tetrahydrocannabinol¹ ((-)-⁹-THC, **1**, Figure 1) and its congeners act at CB1 and CB2,²⁻⁴ two G_{i/o}-protein-coupled cannabinoid receptors that are currently being targeted for various conditions including pain, inflammation, neuro-degeneration, glaucoma, eating and mental disorders, as well as cancer.⁵⁻¹⁴ Owing to the undesirable side effects associated with CB1 receptor activation/deactivation as well as poor pharmacokinetic/pharmacodynamic (PK/PD) properties, only a limited number of cannabinergic drugs have been approved to date.¹⁵ Thus, the development of safer THC-based medications with favorable oral bioavailability, consistent efficacy, and predictable time course of action and detoxification remains to be addressed.

Toward this end, we recently reported on a controlled deactivation/detoxification approach where the “soft” analogue/drug concept of enzymatic deactivation was combined with a “depot effect” that is commonly observed with ⁹-THC and other lipophilic cannabinoids. In our design, the compound’s systemic half-life is determined by two factors. The first reflects the ability of the compound to sequester in some tissue reservoir such as fatty tissue (depot effect). The tissue sequestration affects the availability of the compound for receptor activation as well as for hydrolytic deactivation through systemic circulation. This process is dependent on the compound’s physicochemical properties and can be modulated by adjusting log *P* and PSA. Thus, more lipophilic compounds are slowly released in the bloodstream from the depot while more polar compounds are expected to have less of a depot effect. We have also confirmed that, in the compounds discussed here, the hydrolytic metabolic pathway is the most dominant and is considerably faster than other metabolic options such as reactions involving microsomal enzymes. The second is the rate of enzymatic hydrolysis of a metabolically labile ester group (–C(O)–O–) by blood esterases. This can be calibrated by incorporating suitable stereochemical features in the vicinity of the hydrolyzable moiety (enzymatic effect).¹⁶ Currently, we have developed two controlled-deactivation cannabinergic templates based on the tricyclic classical cannabinoid prototype. In the first, the C-ring in THC was replaced by a hydrolyzable seven-membered lactone,¹⁷ while in the second, the metabolically labile ester group was placed at the 2′-position of the side chain pharmacophore (Figure 1).¹⁶

In the present SAR study, we sought to probe the ester side chain pharmacophore in the (-)-⁸-THC prototype within a novel series of analogues with regard to affinity for the CB1 and CB2 cannabinoid receptors, *in vitro* and *in vivo* potency and efficacy, as well as ability to control the half-lives of deactivation through enzymatic action. An additional goal of this work was to explore the polar characteristics of the side chain and gain information related

to the modulation of the depot effect and its role in the in vivo pharmacokinetic profile of the analogues. The above considerations led us to design ligands that retain the metabolically labile group at the 2'-position of the side chain and replace the ester group ($-\text{C}(\text{O})-\text{O}-$) with the reverse ester ($-\text{O}-\text{C}(\text{O})-$) as well as with the corresponding thioester ($-\text{C}(\text{O})-\text{S}-$) and the hydrolytically more stable amide group ($-\text{C}(\text{O})-\text{NH}-$) (Figure 2). To explore the chain length, we synthesized analogues with four- to nine-atom-long side chains. Additionally, to probe the ligand's polarity, we incorporated bromo-, cyano-, and imidazolyl-groups at the distal side chain carbon atom. As with our previous work,¹⁶ to regulate the rates of enzymatic inactivation while enhancing the compound's affinities for CB receptors, we introduced benzylic substituents contiguous to the metabolically vulnerable ester group.

All novel compounds were characterized by determining their in vitro CB1 and CB2 receptor affinities. Of these, the most interesting were assessed for their functional activities and for their in vitro metabolic stabilities toward mouse plasma esterases while a limited representative set of key compounds was evaluated for their hypothermic and analgesic effects in vivo. Our data show that (-)-⁸-THC analogues carrying five- to nine-atom-long side chains that are substituted with geminal dimethyl and cyclobutyl groups at the C1'-position exhibit remarkably high affinities for the CB1 and CB2 receptors. As predicted, all novel analogues were found to be susceptible to enzymatic deactivation by plasma esterases in a controllable manner, while their metabolites showed no or very low cannabinergic activity. Additionally, all key compounds were shown to be agonists for the CB1 receptor when tested for their abilities to reduce cAMP levels and also produce the characteristic CB1-mediated hypothermia and analgesia in rats and mice. Equally important, in the hypothermia assay, the 6'-cyano-2'-carboxy-⁸-THC analogue **10a** (AM7438) exhibited 10-fold higher potency as well as faster onset and shorter duration of action than the less polar carboxy counterpart **2b**. Also, the offset of the analgesic effect was significantly faster for **10a** compared to **2b**. Congruent with our rational design, these in vivo results suggest that the depot effect of our controlled deactivation analogues can suitably be modulated by enhancing the polar characteristics of the side chain pharmacophore without any significant loss of potency.

CHEMISTRY

Syntheses of the 4'-bromo- and 4'-cyano-butyl esters **6a–6c** and **7a–7c** are summarized in Scheme 1. The required (-)-⁸-THC carboxylic acids **5a–5c** were synthesized from commercially available (3,5-dimethoxyphenyl)acetonitrile and (+)-*cis/trans-p*-mentha-2,8-dien-1-ol in three to four steps following our recently reported procedures.¹⁶ Alkylation of the respective carboxylate anions with 1,4-dibromobutane under microwave heating led to the corresponding esters **6a–6c** in 45–63% yields.¹⁶ Treatment of these bromides with sodium cyanide in dimethyl sulfoxide¹⁸ produced the respective side chain cyano-substituted analogues **7a–7c** in 54–71% yields.

In a similar fashion, the tricyclic carboxylic acid **5b** was transformed to the side chain homologues **8a**, **8b**, and **9a–9d** in 47–87% yields (Scheme 2). Reaction of the 3-bromopropyl ester **9b** with sodium cyanide or imidazole in the presence of potassium carbonate, in

dimethyl sulfoxide, led to the end carbon substituted derivatives **10a** and **10b** (41–98% yields).

Synthesis of the reverse ester analogue **16** involves a Mitsunobu esterification reaction¹⁹ as the key step (Scheme 3). Thus, reduction of nitrile **11** with diisobutylaluminum hydride²⁰ at $-78\text{ }^{\circ}\text{C}$ led to aldehyde **12** (92% yield), which upon exposure to sodium borohydride in methanol²¹ afforded the respective alcohol **13** in excellent yield (94%). Cleavage of the methyl ether groups in **13** using boron tribromide¹⁸ produced resorcinol **14** in 47% yield. Acid catalyzed condensation of this intermediate with chiral terpenoid alcohol **17** in refluxing chloroform for 4–6 h gave (–)- δ -THC alcohol **15** in 21% isolated yield along with unidentified byproducts. We were able to improve this yield (28%) using microwave conditions over a much shorter time period (10 min).¹⁶ Subsequently, Mitsunobu esterification of **15** with *n*-valeric acid using triphenylphosphine and diethyl azodicarboxylate led to the final ester **16** (41% yield).

Treatment of the α,α -dimethyl-carboxylic acid **5b** with [bis(2-methoxyethyl)amino]sulfur trifluoride and coupling of the in situ generated acyl fluoride²² with *n*-pentylamine afforded the (–)- δ -THC amide **18** in 70% yield (Scheme 4). Exposure of the same starting material (**5b**) to the benzotriazole/thionyl chloride reagent²³ followed by treatment of the intermediate acyl chloride **19** with *n*-propanethiol led to thioester **20** in 23% yield for the two steps.

CANNABINOID RECEPTOR AFFINITIES

The abilities of compounds **6a–6c**, **7a–7c**, **8a**, **8b**, **9a–9d**, **10a**, **10b**, **15**, **16**, **18**, and **20** to displace the radiolabeled CB1/CB2 agonist CP-55,940 from membranes prepared from rat brain (source of CB1) and HEK293 cells expressing either mouse CB2 or human CB2 were determined as described earlier,^{18,20} and inhibition constant values (K_i) from the respective competition binding curves are listed in Table 1 in which our prototype (–)- δ -THC, as well as the first-generation carboxy- δ -THCs **2a–2c** are included for comparison. The rat, mouse, and human CB1 receptors have 97–99% sequence identity across species and, as shown earlier,¹⁶ are not expected to exhibit variations in their K_i values. However, mouse CB2²⁴ (mCB2) exhibits only 82% sequence identity with the human clone³ (hCB2). This divergent nature of mCB2 and hCB2 receptors was shown in earlier work^{25,26} to be associated with species-based differences in affinity. For this reason, the analogues were also tested on hCB2.

The compounds included in this study are (–)- δ -THC analogues in which a four- to nine-atom-long side chain with or without 1'-substituents incorporates an enzymatically vulnerable group at the 2'- or 3'-positions. Optimization of the novel carboxy or thiocarboxy-ester side chains was probed through the synthesis of analogues carrying bromo-, cyano-, and imidazolyl-substituents at the distal carbon atom. As predicted based on our earlier results, the hydrolytic metabolites **5a–5c** and **15** have no significant affinities for CB1 and CB2 receptors, thus minimizing the possibility of undesirable cannabinoid receptor related side effects. Comparison of the binding data of (–)- δ -THC and its carboxyester congeners **2a**, **6a**, and **7a** suggests that extension of the linear chain from five to seven–nine

atoms, along with incorporation of an ester group at the 2',3'-positions, enhances the binding affinities of these analogues for both the CB1 and CB2 receptors. We also observed that incorporation of the bromo as well as the more polar cyano substituents at the terminal carbon of the side chain is well tolerated. Comparison of the binding data of our prototype (-)-⁸-THC and compound **8b** demonstrates the remarkable effects of 1',1'-dimethyl-2'-carboxyester substitution (-C(CH₃)₂-C(O)O-) on the side chain pharmacophore. Thus, **8b** with the five-atom-long side chain exhibits 10-, 78-, and 24-fold higher binding affinities for rCB1, mCB2, and hCB2 receptors, respectively, when compared to (-)-⁸-THC. The one-carbon shorter homologue **8a** has significantly reduced affinities for both CB receptors, indicating that a minimum requirement for substantial affinity for both receptors in this series is a five-atom-long side chain. This high affinity can be maintained all through side chain lengths of nine atoms with or without terminal bromine substituents (analogues **2b**, **6b**, and **9a-c**). Interestingly, this holds true when the terminal two or three atoms of the chain are replaced by the polar cyano group or the bulkier and amphiprotic imidazole ring (compounds **10a**, **10b** and **7b**). Notably, the cyano analogues **10a** and **7b** exhibit remarkably high affinities for the CB1 and CB2 receptors. However, extension of the ω -substituted imidazolyl chain of **10b** by one methylene group (compound **9d**) results in a reduction of the ligand's affinity for both cannabinoid receptors, an effect more accentuated in CB1 (~8-fold reduction). Taken together, these data suggest that the pharmacophoric limits for an ω -substituted 1',1'-dimethyl-2'-carboxyester chain could not be extended beyond the nine atoms.

A comparison of the binding affinities of the nonsubstituted analogues **6a** and **7a** with their respective *gem*-dimethyl counterparts **6b** and **7b** shows that introduction of two methyl substituents at the 1'-position of an ω -substituted carboxylated chain leads to an enhancement (20-fold maximum) in CB1 and CB2 receptor affinities. This increase in the ligand's affinities for both CB1 and CB2 receptors holds true when the *gem*-dimethyl substitution is modified to the bulkier cyclobutyl ring (analogues **6c** and **7c**). An examination of the binding data of the 2',3'-carboxyester analogue **2b** and its sulfur and nitrogen congeners **18** and **20** shows that the ester moiety (-C(O)-O-) can be replaced by the respective thioester (-C(O)-S-) and amide (-C(O)-NH-) groups. Likewise, analogue **16** incorporating the sterically less hindered retro ester group (-O-C(O)-) at the 3',4'-position maintains high affinity for both the CB1 and CB2 receptors.

In summary, the detailed SAR reported here shows that a five- to nine-atom-long side chain with *gem*-dimethyl or cyclobutyl substituents at the 1'-position and an enzymatically vulnerable group within the 2' or 3' chain segment results in analogues with remarkably high affinities for both CB1 and CB2 receptors. Importantly, addition of the bromo- or cyano-groups as well as the bulky and amphiprotic imidazole ring at the terminal carbon maintains or enhances the affinity of the ligand for the CB receptors.

IN VITRO PLASMA STABILITY STUDIES

Representative analogues within this series were assessed for their in vitro plasma stability toward mouse plasma esterases as detailed in the Experimental Section.^{16,17} It should be noted that blood contains various esterases which play the major role in the hydrolysis of

compounds carrying ester, carbamate, or phosphate bonds. These esterases include acetylcholinesterases (ACHE), butyrylcholinesterases (BCHE), paraoxonases, and carboxyesterases (in mice and rat but not in human plasma). Esterase activity can be found mainly in plasma, with less activity in red blood cells. Plasma albumin itself may also act as an esterase under certain conditions. For example, albumin contributes about 20% of the total hydrolysis of aspirin to salicylic acid in human plasma. The esterase activity in blood seems to be more extensive in small animals such as rats than in large animals and humans.²⁷ A comparison of the half-lives ($t_{1/2}$, Table 1) of the alkyl bromide and nitrile having no substitution at the 1'-position (**6a**, **7a**) with their 1'-gem-dimethyl (**6b**, **7b**) and 1'-cyclobutyl (**6c**, **7c**) counterparts shows that the plasma esterase stabilities of the analogues correlate well with the presence and the size of 1'-substituents. Thus, the order of metabolic stabilities for the bromo- and cyano-substituted analogues is **6a** < **7a** < **6b** < **7b** < **6c** < **7c**, with the compounds carrying the bulkier cyclobutyl group being the most hydrolytically stable. This trend with the ω -substituted eight- to nine-atom-long side chain analogues parallels our earlier observations with the shorter (seven-atoms) and unsubstituted side chain congeners **2a**, **2b**, and **2c**.¹⁶ Another general observation through this structure–stability relationship study is that regardless of the 1'-substituent, addition of a bromo- or cyano-group at the terminal carbon of a seven-atom-long chain increases its stability toward esterases with the cyano-substituted chain exhibiting the highest stability (comparison of **2a** with **6a** and **7a**, **2b** with **6b** and **7b**, and **2c** with **6c** and **7c**).

The effect of ω -substitution on the chain's enzymatic stability profile was studied in more detail in the 1'-gem-dimethyl series through the assessment of the half-lives of the cyano- and imidazolyl-substituted analogues **10a**, **10b**, **7b**, and **9d**. We observe that presence of a terminal cyano group or the larger imidazole ring reduce the enzymatic lability of the 1'-gem-dimethyl chain (analogue **2b**) by 3- to 31-fold. As expected, the sterically less hindered retro ester analogue **16** was more prone to enzymatic hydrolysis when compared to the α,α -dimethyl-carboxylated counterpart **2b**, while the amide group (**18**) was shown to have remarkable plasma stability. In agreement with earlier work on the rates of hydrolysis of ethyl butyrate and ethyl thiobutyrate by pig liver esterases,²⁸ the thioester **20** exhibits higher stability in mouse plasma esterases than the respective oxoester **2b**. Overall, our data show that the rate of enzymatic inactivation of our side chain carboxyester ⁸-THCs can be controlled by (1) structural features in the vicinity of the hydrolyzable group and (2) substituents at the terminal carbon.

FUNCTIONAL CHARACTERIZATION

Functional characterization of key compounds for the rCB1 receptor was carried out by measuring the decrease in forskolin-stimulated cAMP, as detailed earlier.^{16,18} Compounds were initially screened in three different concentrations (three-point data), and the approximate EC₅₀ values were calculated (Table 2). Subsequently, the accurate EC₅₀ value of the most potent analogue **10a** was determined from two independent experiments (eight-point data) and listed in Table 2 along with data for the related compounds **2b** and **2c** for comparison. We observe that all tested analogues are full agonists at the CB1 receptor while their EC₅₀ values correlate well with their respective binding affinities. Of the compounds tested, the carboxyester ⁸-THC analogues **2b** and **2c** as well as their ω -substituted cyanide

congener **10a** were found to be the most potent and efficacious compounds within the series with EC₅₀s of 0.5, 0.4, and 0.9 nM, respectively.

MOLECULAR MODELING

As an aid in the interpretation of the data, we carried out conformational analyses and docking studies (detailed procedures are given under Experimental Section) involving our lead analogue **10a**, the nonhydrolyzable counterpart (-)-⁸-THC-DMH as well as the parent compound (-)-⁸-THC.

Conformational Analysis

Initial conformational analyses of (-)-⁸-THC, (-)-⁸-THC-DMH, and **10a** revealed a difference in the conformation of the side chains in their global minimum energy conformers. Both (-)-⁸-THC-DMH and **10a** have their side chains oriented orthogonal to the phenol ring, while for (-)-⁸-THC, the five-carbon side chain extends in the same plane as its phenol ring. Initial in vacuo conformational analyses of **10a** identified an intramolecular hydrogen bond between the cyano nitrogen and the phenolic hydroxyl. The **10a** phenolic hydroxyl to cyano nitrogen hydrogen bond heteroatom distance (N–O) and hydrogen bond (O–H–N) angle were 3.22 Å and 144°, respectively. The intramolecular hydrogen bond in **10a** was not found in the global minimum energy conformation from a second conformational search performed using the OPAL2005 force field with an implicit GB/SA solvent model for water. Preliminary results from a 70 ns NAMD molecular dynamics simulation of **10a** in a fully hydrated POPC lipid bilayer found a very low incidence of this internal hydrogen bond as well (unpublished data). For this reason, the nearest low energy conformer without an intramolecular hydrogen bond (which was 1.77 kcal/mol above the initial global min) was used for the calculation of conformational energy costs for **10a**. The first and second side chain dihedrals of this conformer compare well with the global minimum energy conformer of (-)-⁸-THC-DMH, shown in Table 3. Finally, the phenolic hydroxyls of all three ligands were found to prefer the proton directed toward the C2 phenyl ring position nearer the side chain and with the value of the C2–C1–O1–H1 dihedral near zero. A comparison of the lowest energy conformation of **10a** without the internal hydrogen bond to those of (-)-⁸-THC-DMH and (-)-⁸-THC is shown in Figure 3.

Docking Studies

To provide a representation for the interaction of the above three compounds with the hCB1 receptor, we carried out docking studies with an activated form of a CB1 receptor model and calculated relative ligand/receptor interaction energies. Glide docking studies of **10a** in the activated CB1 receptor revealed a significant role for the ester group at the 2' position. The carbonyl oxygen within the ester group has a hydrogen bonding interaction with T3.33(197) as shown in Figure 4A. The hydrogen bond heteroatom distance (O–O) and hydrogen bond (O–H–O) angle are 2.56 Å and 165°, respectively. The T3.33(197) hydrogen bonding interaction is not available to the (-)-⁸-THC-DMH counterpart or the parent compound (-)-⁸-THC as shown in parts B and C of Figure 4. However, all three compounds modeled in the Glide docking studies have a phenolic hydroxyl that interacts directly with K3.28(192). The K3.28(192) and **10a** phenolic hydroxyl hydrogen bond heteroatom distance

(N–O) and hydrogen bond (N–H–O) angle are 2.73 Å and 170°, respectively. The K3.28(192) and (–)-⁸-THC-DMH phenolic hydroxyl hydrogen bond heteroatom distance (N–O) and hydrogen bond (N–H–O) angle are 2.69 Å and 171°, respectively. Finally, the K3.28(192) and (–)-⁸-THC phenolic hydroxyl hydrogen bond heteroatom distance (N–O) and hydrogen bond (N–H–O) angle are 2.64 Å and 168°, respectively.

Glide XP scores adjusted for ligand strain reflect the rank order of K_i s (Table 3) in rCB1 with (**10a** = –5.7 kcal/mol) \approx ((–)-⁸-THC-DMH = –5.4 kcal/mol) < ((–)-⁸-THC = –4.1 kcal/mol). For a list of Glide XP scores in rank order and adjusted by ligand conformational cost, see Supporting Information, Tables S2–S4. A breakdown of ligand/receptor interaction energies revealed the importance of van der Waals interactions for each of ligands and how the two 1',1'-dimethyl analogues (**10a** and (–)-⁸-THC-DMH) have far more of these interactions than (–)-⁸-THC. The (–)-⁸-THC-DMH and **10a** have nine and eight van der Waals interactions better than –2.0 kcal/mol, respectively, while (–)-⁸-THC has five such interactions. The most important van der Waals interactions in common for the 1',1'-dimethyl analogues are F3.25(189), L3.29(193), F(268), M6.55(363), M(371), S7.39(383), and C7.42(386). The (–)-⁸-THC parent interacts in a likewise manner with only F3.25(189), L3.29(193), F(268), M(371), and S7.39(383). Of these residues, L3.29(193), F(268), M6.55(363), and M(371) form part of a tunnel-shaped hydrophobic enclosure between TMHs 3 and 6 for the side chain of each analogue to occupy. Unique to **10a** is the van der Waals interaction with V3.32(196), and unique to (–)-⁸-THC-DMH is F7.35(329). A full listing of all ligand/receptor interaction energies is given in the Supporting Information, Tables 5–7.

Total ligand/receptor interaction energies also follow the trend of the Glide XP scores and K_i s in rCB1 with (**10a** = –42.9 kcal/mol) \approx ((–)-⁸-THC-DMH = –44.4 kcal/mol) < ((–)-⁸-THC = –35.6 kcal/mol). The docked conformational cost for each ligand after the post Glide minimization (**10a**, 0.18 kcal/mol; (–)-⁸-THC-DMH, 0.28 kcal/mol; and (–)-⁸-THC, 0.13 kcal/mol) was small. Compound **10a** did not have a statistically significant lower K_i compared to (–)-⁸-THC-DMH, even though Glide docking studies identified two hydrogen bonds for **10a** compared to one hydrogen bond for (–)-⁸-THC-DMH. This may be due to the energetic cost for **10a** to place its hydrophilic ester and cyano moieties in a generally hydrophobic pocket in the CB1 receptor. This cost likely causes the two K_i s to be essentially equivalent.

IN VIVO BEHAVIORAL CHARACTERIZATION

Representative analogues within this series were initially screened using the hypothermia test in rats (data not shown), and the order of the potency was found to be **10a** > **7b** **6b** > **2b** \approx **20** **16** \approx **8b** **18**. Subsequently, the most promising compound **10a** was studied in more detail and its in vivo hypothermic and antinociceptive profiles were compared to those of the earlier analogue **2b** as well as with the nonhydrolyzable parent compound (–)-⁸-THC-DMH.

Hypothermia Testing

Body temperature was measured in isolated rats over a 6 h period following drug injection (detailed procedures are given in the Experimental Section). Compound **10a** decreased core body temperature in a dose-dependent manner, with a dose of 0.1 mg/kg reducing body temperature up to 4.5 ± 0.5 °C from an average baseline of 37.8 ± 0.1 °C (Figure 5). Its ED₅₀ value (i.e., the dose required to reduce temperature by 3 °C) was 0.034 mg/kg (95% CI: 0.026, 0.041 mg/kg). For comparison, the effects of our first-generation analogue **2b** and those of the (–)-⁸-THC-DMH are also shown. The ED₅₀ values were 0.37 (0.14, 0.73 with 95% CI) for **2b** and 0.29 (0.18, 0.45 with 95% CI) for (–)-⁸-THC-DMH. Thus, **10a** is approximately 8–10-fold more potent than (–)-⁸-THC-DMH and **2b**. Limited extended studies comparing hypothermia induced by equipotent doses of the 6'-cyano-2'-carboxy-⁸-THC analogue **10a** and its structurally related analogues **2b** and (–)-⁸-THC-DMH for 12 h provided an estimate of their in vivo times of action. Thus, at a dose of 0.03 mg/kg, near its ED₅₀ value, compound **10a** reduced body temperature by 2 °C within 3 h of injection and these effects were not observed 6 h after injection (see Supporting Information, Figure S1). This was compared with the effects of equivalent doses (near their ED₅₀ values) of **2b** and (–)-⁸-THC-DMH. Thus, for **2b**, a dose of 0.3 mg/kg produced effects that persisted for at least 6 h after injection while a dose of 0.3 mg/kg of (–)-⁸-THC-DMH produced an equivalent reduction in temperature beyond 12 h after injection. It should be noted that in order to compare equiactive doses of the most potent compound **10a** with those of the in vivo less potent (–)-⁸-THC-DMH and **2b**, we have used different doses of the three drugs that are consistent with their ED₅₀ values. Our data indicate that the depot effect as reflected in the log *P* and PSA values (Table 4) plays the most dominant role in determining the in vivo hypothermic half-lives of compounds **10a**, **2b**, and the nonhydrolyzable (–)-⁸-THC-DMH. Thus, notwithstanding the shorter in vitro hydrolytic half-life of compound **2b**, when compared to **10a**, this compound has a longer in vivo half-life. These results are represented in Table 4.

Analgesia Testing

The pharmacokinetic profiles of analogues bearing the carboxyester (**2b**) and the more polar cyano-carboxyester (**10a**) side chains were further studied in the CB1 receptor-characteristic analgesia test in mice, and the results are depicted in Figure 6 (the dose response graph for four doses of **10a** are given under Supporting Information, Figure S2). A mixed model repeated measures ANOVA (IBM software package SPSS, v.21) applied to the tail-flick latency data produced by compounds **10a** and **2b** during the descending phase (180 and 360 min) showed significant main effects for drug (D) ($F_{1,44} = 8.98$; $p = 0.004$), dose-level (L) ($F_{1,44} = 40.95$; $p = 0.001$), and time (T) ($F_{1,44} = 28.46$; $p = 0.001$). Of more interest, however, is that pairwise comparisons within these parameters (D, L, and T) using Sidak multiple comparison *t* test procedure suggested significant differences for all three parameters ($p = 0.05$). Thus, the tail-flick latencies were dose- and time-dependent for both compounds in a similar manner, and because the pairwise comparison for drug was also significant, the offset of the analgesia effect was significantly faster for **10a** compared to **2b**. The average (\pm SEM) baseline tail-flick withdrawal latency for all mice ($N = 24$) examined with compound **10a** was 0.99 ± 0.05 s.

Overall, our in vivo experiments show that in rats, compound **10a** is approximately a 10–30-fold more potent as a cannabinoid agonist when compared to **2b** and (–)-⁸-THC-DMH. Also, this more potent analogue has a faster onset and shorter duration of action when compared to the less polar counterpart **2b** and the lipophilic and nonhydrolyzable parent compound (–)-⁸-THC-DMH. Our antinociception data in mice clearly show that the cyano-carboxyl-analogue **10a** has a shorter duration of action than its congener with no cyano substitution (**2b**).

CONCLUSIONS

In summary, as a continuation of our earlier work on the controlled deactivation/detoxification ligand development project, we sought to probe the novel carboxyester side chain pharmacophore in (–)-⁸-THCs for CB receptor binding affinity, in vitro and in vivo potency and efficacy, as well as its effects on the half-lives of deactivation through enzymatic activity. We have also explored the chain's polar characteristics that are associated with the depot effect, in an effort to produce cannabinoids with faster onset/offset and shorter duration of action than the currently existing (–)-⁸-THC analogues. In connection with our earlier work where we focused on the chain's benzylic position and the related subsite within the receptor's binding domain,^{18,20,29–33} the current SAR study extends the mapping of the chain's pharmacophoric space beyond the 1'-carbon and argues that both CB receptors can tolerate polar groups and atoms within the second and the fourth position of the chain. We are hopeful that these observations will provide us with new opportunities for the design of high affinity/efficacy novel analogues with improved selectivities for the two cannabinoid receptors. The most successful compound identified through this careful study, namely 2-[(6a*R*,10a*R*)-6a,7,10,10a-tetrahydro-1-hydroxy-6,6,9-trimethyl-6*H*-dibenzo[*b,d*]pyran-3-yl]-2-methyl-propanoic acid 3-cyano-propyl ester (**10a**), is a remarkably potent and efficacious CB1 receptor agonist with relatively shorter duration of action than its less polar 2'-carboxy-(–)-⁸-THC-DMH counterpart and the highly lipophilic and long lasting (–)-⁸-THC-DMH. Our data support the hypothesis that the pharmacological half-lives of our selectively detoxified analogues can be controlled by the joint modulation of their relative stabilities for plasma esterases as well as through variation of their polar characteristics and thus to the depot effects.

EXPERIMENTAL SECTION

Materials

All reagents and solvents were purchased from Aldrich Chemical Co., unless otherwise specified, and used without further purification. All anhydrous reactions were performed under a static argon atmosphere in flame-dried glassware using scrupulously dry solvents. Flash column chromatography employed silica gel 60 (230–400 mesh). All compounds were demonstrated to be homogeneous by analytical TLC on precoated silica gel TLC plates (Merck, 60 F₂₄₅ on glass, layer thickness 250 μm), and chromatograms were visualized by phosphomolybdic acid staining. Melting points were determined on a micromelting point apparatus and are uncorrected. IR spectra were recorded on a PerkinElmer Spectrum One FT-IR spectrometer. NMR spectra were recorded in CDCl₃, unless otherwise stated, on a Bruker Ultra Shield 400 WB plus (¹H at 400 MHz, ¹³C at 100 MHz) or on a Varian

INOVA-500 (^1H at 500 MHz, ^{13}C at 125 MHz) spectrometers, and chemical shifts are reported in units of δ relative to internal TMS. Multiplicities are indicated as br (broadened), s (singlet), d (doublet), t (triplet), q (quartet), and m (multiplet), and coupling constants (J) are reported in hertz (Hz). Low and high-resolution mass spectra were performed in School of Chemical Sciences, University of Illinois at Urbana–Champaign. Mass spectral data are reported in the form of m/z (intensity relative to base = 100). Elemental analyses were obtained in Baron Consulting Co, Milford, CT, and were within $\pm 0.4\%$ of the theoretical values (see Supporting Information). Purities of the tested compounds were determined by elemental analysis or by HPLC (using Waters Alliance HPLC system, 4.6 mm \times 250 mm, Supelco Discovery column, acetonitrile/water with 8.5% *o*-phosphoric acid) or by LC/MS analysis using a Waters MicroMass ZQ system (electrospray ionization (ESI) with Waters-2525 binary gradient module coupled to a photodiode array detector (Waters-2996) and ELS detector (Waters-2424) using a XTerra MS C18 (5 μm , 4.6 mm \times 50 mm column and acetonitrile/water) and were $>95\%$.

2-[(6aR,10aR)-6a,7,10,10a-Tetrahydro-1-hydroxy-6,6,9-trimethyl-6H-dibenzo[b,d]pyran-3-yl]acetic Acid 4-Bromo-butyl Ester (6a)—

A stirred mixture of **5a** (175 mg, 0.58 mmol), dibromobutane (313 mg, 1.45 mmol), and sodium bicarbonate (73 mg, 0.87 mmol) in DMF (2 mL) was heated at 165 $^\circ\text{C}$ for 12 min using microwave irradiation. The reaction mixture was cooled to room temperature and diluted with water and ethyl acetate. The organic layer was separated, and the aqueous phase was extracted with ethyl acetate. The combined organic layer was washed with brine, dried (MgSO_4), and concentrated under reduced pressure. Purification by flash column chromatography on silica gel gave **6a** (159 mg, 63% yield) as a light-yellow gum. IR (CHCl_3): 3407, 2967, 2928, 1712 (s, $>\text{C}=\text{O}$), 1621, 1583, 1431, 1254 cm^{-1} . ^1H NMR (500 MHz, CDCl_3) δ 6.33 (d, J = 1.0 Hz, 1H, 4-H), 6.24 (d, J = 1.0 Hz, 1H, 2-H), 5.42 (m as d, J = 4.0 Hz, 1H, 8-H), 5.23 (s, 1H, OH), 4.12 (t, J = 6.5 Hz, 2H, $-\text{OCH}_2-$), 3.45 (s, 2H, $-\text{CH}_2-\text{C}(\text{O})\text{O}-$), 3.39 (t, J = 6.5 Hz, 2H, $-\text{CH}_2\text{Br}$), 3.19 (dd, J = 15.0 Hz, J = 4.5 Hz, 1H, 10 α -H), 2.69 (td, J = 11.0 Hz, J = 4.5 Hz, 1H, 10 α -H), 2.19–2.10 (m, 1H, 7 α -H), 1.94–1.76 (m, 7H, 10 β -H, 7 β -H, 6 α -H, $-\text{CH}_2-\text{CH}_2-\text{Br}$, $-\text{CH}_2-\text{CH}_2-\text{CH}_2-\text{Br}$), 1.69 (s, 3H, 9- CH_3), 1.37 (s, 3H, 6 β - CH_3), 1.09 (s, 3H, 6 α - CH_3). Mass spectrum (EI) m/z (relative intensity) 438 ($\text{M}^+ + 2$, 97), 436 (M^+ , 97), 395 (38), 393 (38), 355 (95), 353 (95), 330 (60), 316 (38), 287 (46), 273 (48), 257 (45), 247 (98), 233 (60), 213 (100). Exact mass (EI) calculated for $\text{C}_{22}\text{H}_{29}\text{O}_4\text{Br}$ (M^+), 436.1249; found, 436.1252. HPLC (4.6 mm \times 250 mm, Supelco discovery column, acetonitrile/water) showed purity 97.5% and retention time 12.6 min for the title compound. LC/MS analysis (Waters MicroMass ZQ system) showed purity 97% and retention time 7.3 min for the title compound.

2-[(6aR,10aR)-6a,7,10,10a-Tetrahydro-1-hydroxy-6,6,9-trimethyl-6H-dibenzo[b,d]pyran-3-yl]-2-methyl-propanoic Acid 4-Bromo-butyl Ester (6b)—

The synthesis was carried out as described for **6a** using **5b** (200 mg, 0.61 mmol), dibromobutane (330 mg, 1.53 mmol), and sodium bicarbonate (77 mg, 0.92 mmol) in DMF and gave **6b** (148 mg, 53% yield) as a light-yellow gum. IR (neat): 3403, 2970, 2917, 1727, and 1703 (s, $>\text{C}=\text{O}$), 1620, 1577, 1416, 1256 cm^{-1} . ^1H NMR (500 MHz, CDCl_3) δ 6.41 (d, J = 2.0 Hz, 1H, 4-H), 6.25 (d, J = 2.0 Hz, 1H, 2-H), 5.42 (m as d, J = 5.0 Hz, 1H, 8-H), 5.18

(s, 1H, OH), 4.09 (t, $J = 6.5$ Hz, 2H, $-\text{OCH}_2-$), 3.32 (t, $J = 6.5$ Hz, 2H, $-\text{CH}_2\text{Br}$), 3.19 (dd, $J = 15.0$ Hz, $J = 4.5$ Hz, 1H, $10\alpha\text{-H}$), 2.69 (td, $J = 11.0$ Hz, $J = 4.5$ Hz, 1H, $10\alpha\text{-H}$), 2.18–2.10 (m, 1H, $7\alpha\text{-H}$), 1.85–1.68 (m and s overlapping, 10H, $10\beta\text{-H}$, $7\beta\text{-H}$, $6\alpha\text{-H}$, $-\text{CH}_2\text{-CH}_2-$ of the side chain and 9-CH_3 , especially 1.70 s, 9-CH_3), 1.51 (s, 6H, $-\text{C}(\text{CH}_3)_2-$), 1.38 (s, 3H, $6\beta\text{-CH}_3$), 1.10 (s, 3H, $6\alpha\text{-CH}_3$). ^{13}C NMR (125 MHz, CDCl_3) δ 177.8 ($>\text{C}=\text{O}$), 155.7 (C-1 or C-5), 155.1 (C-5 or C-1), 144.0, 134.9, 119.4, 112.0, 107.1, 105.3, 77.0 (C-6), 64.3 ($-\text{OCH}_2-$), 46.3, 45.0, 35.9, 33.3, 31.7, 29.3, 28.0, 27.7, 27.2, 26.2, 26.2, 23.8, 18.7. Mass spectrum (ESI) m/z (relative intensity) 467 ($\text{M}^+ + 2 + \text{H}$, 100), 465 ($\text{M}^+ + \text{H}$, 100), 285 (30). Exact mass (ESI) calculated for $\text{C}_{24}\text{H}_{34}\text{O}_4\text{Br}$ ($\text{M}^+ + \text{H}$), 465.1640; found, 465.1647. LC/MS analysis (Waters MicroMass ZQ system) showed purity 98% and retention time 7.4 min for the title compound. Anal. ($\text{C}_{24}\text{H}_{33}\text{BrO}_4$) C, H.

1-[(6aR,10aR)-6a,7,10,10a-Tetrahydro-1-hydroxy-6,6,9-trimethyl-6H-dibenzo[b,d]pyran-3-yl]-cyclobutanecarboxylic Acid 4-Bromo-butyl Ester (6c)

—The synthesis was carried out as described for **6a** using **5c** (145.0 mg, 0.42 mmol), dibromobutane (136 mg, 0.63 mmol), and sodium bicarbonate (39 mg, 0.46 mmol) in DMF and gave **6c** (90 mg, 45% yield) as a light-yellow gum. IR (neat): 3407, 2968, 2915, 1728, and 1705 (s, $>\text{C}=\text{O}$), 1622, 1416, 1258 cm^{-1} . ^1H NMR (500 MHz, CDCl_3) δ 6.39 (d, $J = 2.0$ Hz, 1H, 4-H), 6.24 (d, $J = 2.0$ Hz, 1H, 2-H), 5.85 (s, 1H, $-\text{OH}$), 5.42 (m as d, $J = 4.5$ Hz, 1H, 8-H), 4.10 (m, 2H, $-\text{OCH}_2-$), 3.31 (t, $J = 6.5$ Hz, 2H, $-\text{CH}_2\text{Br}$), 3.24 (dd, $J = 16.0$ Hz, $J = 4.0$ Hz, 1H, $10\alpha\text{-H}$), 2.79–2.66 (m, 3H, $10\alpha\text{-H}$, 2H of the cyclobutane ring, overlapping), 2.46 (m as qt, $J = 9.0$ Hz, 2H of the cyclobutane ring), 2.19–2.10 (m, 1H, $7\alpha\text{-H}$), 1.99–1.90 (m, 1H of the cyclobutane ring), 1.89–1.64 (m and s overlapping, 11H, $10\beta\text{-H}$, $7\beta\text{-H}$, $6\alpha\text{-H}$, 1H of the cyclobutane ring, $-\text{CH}_2\text{CH}_2\text{CH}_2\text{Br}$, 9-CH_3 , especially 1.69 s, 9-CH_3), 1.38 (s, 3H, $6\beta\text{-CH}_3$), 1.09 (s, 3H, $6\alpha\text{-CH}_3$). Mass spectrum (ESI) m/z (relative intensity) 501 ($\text{M}^+ + 2 + \text{Na}$, 33), 499 ($\text{M}^+ + \text{Na}$, 33), 479 ($\text{M}^+ + 2 + \text{H}$, 100), 477 ($\text{M}^+ + \text{H}$, 100), 297 (30). Exact mass (ESI) calculated for $\text{C}_{25}\text{H}_{34}\text{O}_4\text{Br}$ ($\text{M}^+ + \text{H}$), 477.1640; found, 477.1636. LC/MS analysis (Waters MicroMass ZQ system) showed purity 97% and retention time 5.6 min for the title compound.

2-[(6aR,10aR)-6a,7,10,10a-Tetrahydro-1-hydroxy-6,6,9-trimethyl-6H-dibenzo[b,d]pyran-3-yl]acetic Acid 4-Cyano-butyl Ester (7a)

—A solution of bromide **6a** (80 mg, 0.18 mmol) and sodium cyanide (88 mg, 1.8 mmol) in anhydrous DMSO (5 mL) was stirred at 50 °C for 3 h under argon. The reaction mixture was cooled to room temperature and diluted with water and ethyl acetate. The organic layer was separated, and the aqueous layer was extracted with ethyl acetate. The combined organic layer was washed with brine, dried (MgSO_4), and evaporated under reduced pressure. Purification by flash column chromatography on silica gel (20% ethyl acetate in hexane) afforded **7a** (50 mg, 71% yield) as a light-yellow gum. IR (neat): 3405, 2926, 2249 (CN), 1732 (s, $>\text{C}=\text{O}$), 1621, 1583, 1431, 1262, 1182 cm^{-1} . ^1H NMR (500 MHz, CDCl_3) δ 6.31 (d, $J = 2.0$ Hz, 1H, 4-H), 6.27 (d, $J = 2.0$ Hz, 1H, 2-H), 5.72 (s, 1H, OH), 5.42 (m as d, $J = 4.0$ Hz, 1H, 8-H), 4.14 (t, $J = 6.0$ Hz, 2H, $-\text{OCH}_2-$), 3.46 (s, 2H, $-\text{CH}_2\text{-C}(\text{O})\text{O}-$), 3.22 (dd, $J = 15.0$ Hz, $J = 4.5$ Hz, 1H, $10\alpha\text{-H}$), 2.69 (td, $J = 11.0$ Hz, $J = 4.5$ Hz, 1H, $10\alpha\text{-H}$), 2.35 (t, $J = 7.0$ Hz, 2H, $-\text{CH}_2\text{CN}$), 2.17–2.09 (m, 1H, $7\alpha\text{-H}$), 1.85–1.70 (m, 7H, $10\beta\text{-H}$, $7\beta\text{-H}$, $6\alpha\text{-H}$, $-\text{CH}_2\text{-CH}_2-$ of the side chain), 1.68 (s, 3H, 9-CH_3), 1.37 (s, 3H, $6\beta\text{-CH}_3$), 1.09 (s, 3H, $6\alpha\text{-CH}_3$). Mass

spectrum (EI) m/z (relative intensity) 383 (M^+ , 32), 368 (10), 340 (12), 315 (8), 300 (40), 279 (13), 213 (38), 205 (29), 97 (38), 83 (41), 69 (71), 57 (100). Exact mass (EI) calculated for $C_{23}H_{29}O_4N$ (M^+), 383.2097; found, 383.2092. LC/MS analysis (Waters MicroMass ZQ system) showed purity 96.5% and retention time 6.8 min for the title compound.

2-[(6aR,10aR)-6a,7,10,10a-Tetrahydro-1-hydroxy-6,6,9-trimethyl-6H-dibenzo[b,d]pyran-3-yl]-2-methyl-propanoic Acid 4-Cyano-butyl Ester (7b)—

The synthesis was carried out as described for **7a** using **6b** (20 mg, 0.04 mmol) and sodium cyanide (21 mg, 0.43 mmol) in anhydrous DMSO and gave **7b** (9.5 mg, 54% yield) as light-yellow gum. IR ($CHCl_3$): 3405, 2973, 2249 (CN), 1727 and 1705 (s, $>C=O$), 1620, 1578, 1417, 1258, 1184 cm^{-1} . 1H NMR (500 MHz, $CDCl_3$) δ 6.41 (d, $J = 2.0$ Hz, 1H, 4-H), 6.26 (d, $J = 2.0$ Hz, 1H, 2-H), 5.42 (m as d, $J = 5.0$ Hz, 1H, 8-H), 5.26 (s, 1H, OH), 4.11 (t, $J = 6.5$ Hz, 2H, $-OCH_2-$), 3.20 (dd, $J = 15.0$ Hz, $J = 4.5$ Hz, 1H, 10α -H), 2.69 (td, $J = 11.0$ Hz, $J = 4.5$ Hz, 1H, 10α -H), 2.28 (t, $J = 6.5$ Hz, 2H, $-CH_2CN$), 2.18–2.10 (m, 1H, 7α -H), 1.87–1.72 (m, 5H, 10β -H, 7β -H, 6a-H, $-CH_2-$ of the side chain), 1.70 (s, 3H, 9- CH_3), 1.68–1.58 (m, 2H, $-CH_2-$ of the side chain), 1.51 (s, 3H, $-C(CH_3)_2-$), 1.50 (s, 3H, $-C(CH_3)_2-$), 1.38 (s, 3H, 6β - CH_3), 1.10 (s, 3H, 6α - CH_3). Mass spectrum (ESI) m/z (relative intensity) 434 ($M^+ + Na$, 10), 412 ($M^+ + H$, 100), 285 (5). Exact mass (ESI) calculated for $C_{25}H_{34}NO_4$ ($M^+ + H$), 412.2488; found, 412.2480. LC/MS analysis (Waters MicroMass ZQ system) showed purity 98% and retention time 6.8 min for the title compound.

1-[(6aR,10aR)-6a,7,10,10a-Tetrahydro-1-hydroxy-6,6,9-trimethyl-6H-dibenzo[b,d]pyran-3-yl]-cyclobutanecarboxylic Acid 4-Cyano-butyl Ester (7c)—

The synthesis was carried out as described for **7a** using **6c** (180 mg, 0.38 mmol) and sodium cyanide (186 mg, 3.8 mmol) in anhydrous DMSO and gave **7c** (100 mg, 63% yield) as light-yellow gum. IR ($CHCl_3$): 3400, 2970, 2250 (CN), 1723 and 1703 (s, $>C=O$), 1619, 1577, 1417, 1268, 1183 cm^{-1} . 1H NMR (500 MHz, $CDCl_3$) δ 6.37 (d, $J = 1.5$ Hz, 1H, 4-H), 6.26 (d, $J = 1.5$ Hz, 1H, 2-H), 5.95 (s, 1H, $-OH$), 5.42 (m as d, $J = 4.0$ Hz, 1H, 8-H), 4.11 (t, $J = 5.5$ Hz, 2H, $-OCH_2-$), 3.26 (dd, $J = 16.5$ Hz, $J = 5.0$ Hz, 1H, 10α -H), 2.79–2.67 (m, 3H, 10α -H, 2H of the cyclobutane ring, overlapping), 2.46 (m, 2H of the cyclobutane ring), 2.26 (t, $J = 7.0$ Hz, 2H, $-CH_2CN$), 2.18–2.10 (m, 1H, 7α -H), 2.00–1.90 (m, 1H of the cyclobutane ring), 1.89–1.71 (m, 6H, 10β -H, 7β -H, 6a-H, 1H of the cyclobutane ring, $-CH_2-$ of the side chain), 1.69 (s, 3H, 9- CH_3), 1.63–1.54 (m, 2H, $-CH_2-$ of the side chain), 1.38 (s, 3H, 6β - CH_3), 1.09 (s, 3H, 6α - CH_3). Mass spectrum (ESI) m/z (relative intensity) 446 ($M^+ + Na$, 50), 424 ($M^+ + H$, 100), 297 (5). Exact mass (ESI) calculated for $C_{26}H_{34}NO_4$ ($M^+ + H$), 424.2488; found, 424.2491. LC/MS analysis (Waters MicroMass ZQ system) showed purity 98% and retention time 4.9 min for the title compound. Anal. ($C_{26}H_{33}NO_4$) C, H.

2-[(6aR,10aR)-6a,7,10,10a-Tetrahydro-1-hydroxy-6,6,9-trimethyl-6H-dibenzo[b,d]pyran-3-yl]-2-methyl-propanoic Acid Methyl Ester (8a)—

The synthesis was carried out as described for **6a** using **5b** (240 mg, 0.73 mmol), iodomethane (260 mg, 1.83 mmol), and sodium bicarbonate (92 mg, 1.09 mmol) in DMF and gave **8a** (160 mg, 64% yield) as a light-yellow gum. IR (neat): 3412, 2962, 2932, 1728, and 1702 (s, $>C=O$), cm^{-1} . 1H NMR (500 MHz, $CDCl_3$) δ 6.41 (d, $J = 2.0$ Hz, 1H, 4-H), 6.26 (d, $J = 2.0$ Hz, 1H, 2-H), 5.75 (s, 1H, OH), 5.42 (m as d, $J = 5.0$ Hz, 1H, 8-H), 3.66 (s, 3H, $-OCH_3$),

3.22 (dd, $J = 15.0$ Hz, $J = 4.5$ Hz, 1H, 10 α -H), 2.69 (td, $J = 11.0$ Hz, $J = 4.5$ Hz, 1H, 10 α -H), 2.19–2.10 (m, 1H, 7 α -H), 1.86–1.74 (m, 3H, 10 β -H, 7 β -H, 6 α -H), 1.69 (s, 3H, 9-CH₃), 1.51 (s, 6H, –C(CH₃)₂–), 1.38 (s, 3H, 6 β -CH₃), 1.11 (s, 3H, 6 α -CH₃). ¹³C NMR (125 MHz, CDCl₃) δ 177.8 (>C=O), 155.4 (C-1 or C-5), 155.1 (C-5 or C-1), 144.4, 135.0, 119.4, 111.9, 107.5, 105.4, 77.1 (C-6), 52.6 (–OCH₃), 46.3, 44.9, 35.9, 31.7, 28.1, 27.8, 26.5, 26.4, 23.8, 18.8. Mass spectrum (EI) m/z (relative intensity) 344 (M⁺, 91), 329 (15), 301 (38), 285 (22), 276 (18), 261 (100), 241 (22), 223 (19). Exact mass (EI) calculated for C₂₁H₂₈O₄ (M⁺), 344.1988; found, 344.1992. HPLC (4.6 mm \times 250 mm, Supelco Discovery column, acetonitrile/water) showed purity 96.5% and retention time 12 min for the title compound. LC/MS analysis (Waters MicroMass ZQ system) showed purity 96.5% and retention time 6.6 min for the title compound.

2-[(6aR,10aR)-6a,7,10,10a-Tetrahydro-1-hydroxy-6,6,9-trimethyl-6H-dibenzo[b,d]pyran-3-yl]-2-methyl-propanoic Acid Ethyl Ester (8b)—The synthesis was carried out as described for **6a** using **5b** (300 mg, 0.91 mmol), iodoethane (356 mg, 2.28 mmol), and sodium bicarbonate (115 mg, 1.37 mmol) in DMF and gave **8b** (283 mg, 87% yield) as a light-yellow gum. IR (neat): 3410, 2959, 2931, 1728, and 1702 (s, >C=O), cm⁻¹. ¹H NMR (500 MHz, CDCl₃) δ 6.41 (d, $J = 1.0$ Hz, 1H, 4-H), 6.28 (d, $J = 1.0$ Hz, 1H, 2-H), 5.74 (s, 1H, OH), 5.42 (m as d, $J = 5.0$ Hz, 1H, 8-H), 4.12 (q, $J = 7.0$ Hz, 2H, –OCH₂–), 3.22 (dd, $J = 15.0$ Hz, $J = 4.5$ Hz, 1H, 10 α -H), 2.69 (td, $J = 11.0$ Hz, $J = 4.5$ Hz, 1H, 10 α -H), 2.19–2.10 (m, 1H, 7 α -H), 1.88–1.75 (m, 3H, 10 β -H, 7 β -H, 6 α -H), 1.69 (s, 3H, 9-CH₃), 1.50 (s, 6H, –C(CH₃)₂–), 1.38 (s, 3H, 6 β -CH₃), 1.19 (t, $J = 7.0$ Hz, 3H, –OCH₂CH₃), 1.10 (s, 3H, 6 α -CH₃). Mass spectrum (EI) m/z (relative intensity) 358 (M⁺, 92), 343 (17), 315 (39), 285 (48), 275 (100), 241 (35). Exact mass (EI) calculated for C₂₂H₃₀O₄ (M⁺), 358.2144; found, 358.2145. LC/MS analysis (Waters MicroMass ZQ system) showed purity 97% and retention time 6.9 min for the title compound.

2-[(6aR,10aR)-6a,7,10,10a-Tetrahydro-1-hydroxy-6,6,9-trimethyl-6H-dibenzo[b,d]pyran-3-yl]-2-methyl-propanoic Acid 2-Bromo-ethyl Ester (9a)—The synthesis was carried out as described for **6a** using **5b** (200 mg, 0.61 mmol), 1,2-dibromoethane (287 mg, 1.53 mmol), and sodium bicarbonate (77 mg, 0.92 mmol) in DMF and gave **9a** (127 mg, 48% yield) as a light-yellow gum. IR (neat): 3405, 2972, 2918, 1725, and 1701 (s, >C=O), 1621, 1577, 1415, 1262 cm⁻¹. ¹H NMR (500 MHz, CDCl₃) δ 6.42 (d, $J = 1.5$ Hz, 1H, 4-H), 6.27 (d, $J = 1.5$ Hz, 1H, 2-H), 5.42 (m as d, $J = 4.0$ Hz, 1H, 8-H), 5.04 (br s, 1H, OH), 4.36 (m as td, $J = 5.5$ Hz, $J = 2.0$ Hz, 2H, –OCH₂–), 3.46 (t, $J = 6.0$ Hz, 2H, –CH₂Br), 3.19 (dd, $J = 15.0$ Hz, $J = 4.5$ Hz, 1H, 10 α -H), 2.69 (td, $J = 11.0$ Hz, $J = 4.5$ Hz, 1H, 10 α -H), 2.18–2.10 (m, 1H, 7 α -H), 1.89–1.72 (m, 3H, 10 β -H, 7 β -H, 6 α -H), 1.70 (s, 3H, 9-CH₃), 1.53 (s, 6H, –C(CH₃)₂–), 1.38 (s, 3H, 6 β -CH₃), 1.10 (s, 3H, 6 α -CH₃). Mass spectrum (EI) m/z (relative intensity) 438 (M⁺ + 2, 68), 436 (M⁺, 68), 395 (22), 393 (22), 355 (67), 353 (67), 285 (44), 241 (45), 59 (100). Exact mass (EI) calculated for C₂₂H₂₉O₄Br (M⁺), 436.1249; found, 436.1250. LC/MS analysis (Waters MicroMass ZQ system) showed purity 98% and retention time 8.5 min for the title compound.

2-[(6aR,10aR)-6a,7,10,10a-Tetrahydro-1-hydroxy-6,6,9-trimethyl-6H-dibenzo[b,d]pyran-3-yl]-2-methyl-propanoic Acid 3-Bromo-propyl Ester (9b)—

The synthesis was carried out as described for **6a** using **5b** (405 mg, 1.23 mmol), 1,3-dibromopropane (622 mg, 3.08 mmol), and sodium bicarbonate (155 mg, 1.85 mmol) in DMF and gave **9b** (282 mg, 51% yield) as a light-yellow gum. IR (neat): 3401, 2973, 2917, 1727, and 1703 (s, >C=O), 1621, 1576, 1416, 1260 cm^{-1} . ^1H NMR (500 MHz, CDCl_3) δ 6.41 (d, $J = 1.5$ Hz, 1H, 4-H), 6.27 (d, $J = 1.5$ Hz, 1H, 2-H), 5.89 (s, 1H, OH), 5.42 (m as d, $J = 5.0$ Hz, 1H, 8-H), 4.19 (m as td, $J = 6.5$ Hz, $J = 1.5$ Hz, 2H, $-\text{OCH}_2-$), 3.30–3.18 (t and dd overlapping, 3H, $-\text{CH}_2\text{Br}$, 10 α -H, especially 3.24, t, $J = 6.5$ Hz, 2H, $-\text{CH}_2\text{Br}$), 2.69 (td, $J = 11.0$ Hz, $J = 4.5$ Hz, 1H, 10 α -H), 2.18–2.10 (m, 1H, 7 α -H), 2.09 (qt, $J = 6.5$ Hz, 2H, $-\text{CH}_2\text{CH}_2\text{Br}$), 1.87–1.74 (m, 3H, 10 β -H, 7 β -H, 6 α -H), 1.69 (s, 3H, 9- CH_3), 1.51 (s, 6H, $-\text{C}(\text{CH}_3)_2-$), 1.39 (s, 3H, 6 β - CH_3), 1.11 (s, 3H, 6 α - CH_3). Mass spectrum (ESI) m/z (relative intensity) 453 ($\text{M}^+ + 2 + \text{H}$, 55), 450 ($\text{M}^+ + \text{H}$, 55), 285 (100). LC/MS analysis (Waters MicroMass ZQ system) showed purity 96% and retention time 7.6 min for the title compound. Anal. ($\text{C}_{23}\text{H}_{31}\text{BrO}_4$) C, H.

2-[(6aR,10aR)-6a,7,10,10a-Tetrahydro-1-hydroxy-6,6,9-trimethyl-6H-dibenzo[b,d]pyran-3-yl]-2-methyl-propanoic Acid 5-Bromo-pentyl Ester (9c)—

The synthesis was carried out as described for **6a** using **5b** (350 mg, 1.06 mmol), 1,5-dibromopentane (609 mg, 2.65 mmol), and sodium bicarbonate (134 mg, 1.59 mmol) in DMF and gave **9c** (239 mg, 47% yield) as a light-yellow gum. IR (CHCl_3): 3408, 2973, 2931, 1728, and 1702 (s, >C=O), 1621, 1578, 1417, 1261 cm^{-1} . ^1H NMR (500 MHz, CDCl_3) δ 6.42 (d, $J = 2.0$ Hz, 1H, 4-H), 6.25 (d, $J = 2.0$ Hz, 1H, 2-H), 5.42 (m as d, $J = 5.0$ Hz, 1H, 8-H), 5.07 (s, 1H, OH), 4.03 (t, $J = 6.5$ Hz, 2H, $-\text{OCH}_2-$), 3.29 (t, $J = 6.5$ Hz, 2H, $-\text{CH}_2\text{Br}$), 3.19 (dd, $J = 15.0$ Hz, $J = 4.5$ Hz, 1H, 10 α -H), 2.69 (td, $J = 11.0$ Hz, $J = 4.5$ Hz, 1H, 10 α -H), 2.18–2.10 (m, 1H, 7 α -H), 1.84–1.67 (m and s overlapping, 10H, 10 β -H, 7 β -H, 6 α -H, $-\text{CH}_2-\text{CH}_2-$ of the side chain and 9- CH_3 , especially 1.70 s, 9- CH_3), 1.51 (s, 6H, $-\text{C}(\text{CH}_3)_2-$), 1.38 (s, 3H, 6 β - CH_3), 1.28–1.23 (m, 2H, $-\text{CH}_2-$ of the side chain), 1.10 (s, 3H, 6 α - CH_3). Mass spectrum (EI) m/z (relative intensity) 480 ($\text{M}^+ + 2$, 2), 478 (M^+ , 2), 398 ($\text{M}^+ - \text{Br}$, 82), 355 (19), 330 (21), 315 (100), 285 (60), 241 (39). Exact mass (EI) calculated for $\text{C}_{25}\text{H}_{35}\text{O}_4\text{Br}$ (M^+), 478.1719; found, 478.1715. LC/MS analysis (Waters MicroMass ZQ system) showed purity 96% and retention time 7.5 min for the title compound.

2-[(6aR,10aR)-6a,7,10,10a-Tetrahydro-1-hydroxy-6,6,9-trimethyl-6H-dibenzo[b,d]pyran-3-yl]-2-methyl-propanoic Acid 4-(1H-Imidazol-1-yl)butyl Ester (9d)—

The synthesis was carried out as described for **6a** using **5b** (900 mg, 2.72 mmol), 4-(1H-imidazol-1-yl)butyl bromide (1.12 g, 5.44 mmol), and sodium bicarbonate (343 mg, 4.08 mmol) in DMF and gave **9d** (579 mg, 47% yield) as a light-yellow solid, mp 73–75 $^\circ\text{C}$. IR (CHCl_3): 2971, 2932, 1727 (s, >C=O), 1618, 1578, 1512, 1417, 1251 cm^{-1} . ^1H NMR (500 MHz, CDCl_3) δ 7.50 (s, 1H, imidazole), 7.10 (s, 1H, imidazole), 6.86 (s, 1H, imidazole), 6.35 (d, $J = 2.0$ Hz, 1H, 4-H), 6.23 (d, $J = 2.0$ Hz, 1H, 2-H), 5.41 (m as d, $J = 5.0$ Hz, 1H, 8-H), 3.95 (m as td, $J = 6.5$ Hz, $J = 2.0$ Hz, 2H, $-\text{OCH}_2-$), 3.88 (m as td, $J = 7.5$ Hz, $J = 3.0$ Hz, 2H, $-\text{CH}_2-\text{N}<$), 3.37 (dd, $J = 15.0$ Hz, $J = 4.5$ Hz, 1H, 10 α -H), 2.72 (td, $J = 11.0$ Hz, $J = 4.5$ Hz, 1H, 10 α -H), 2.18–2.09 (m, 1H, 7 α -H), 1.84–1.68 (m and s overlapping, 10H, 10 β -H, 7 β -H, 6 α -H, $-\text{CH}_2-\text{CH}_2-$ of the side chain and 9- CH_3 , especially 1.70 s, 9- CH_3), 1.47 (s, 3H, $-\text{C}(\text{CH}_3)_2-$), 1.46 (s, 3H, $-\text{C}(\text{CH}_3)_2-$), 1.38 (s, 3H, 6 β - CH_3), 1.09 (s, 3H, 6 α - CH_3). Mass spectrum (EI) m/z (relative intensity) 452 (M^+ , 100), 437 (20), 402 (48), 367

(56), 318 (23), 303 (38), 265 (31), 91 (18). Exact mass (EI) calculated for $C_{27}H_{36}N_2O_4$ (M^+), 452.2675; found, 452.2666. Anal. ($C_{27}H_{36}N_2O_4$) C, H, N.

2-[(6aR,10aR)-6a,7,10,10a-Tetrahydro-1-hydroxy-6,6,9-trimethyl-6H-dibenzo[b,d]pyran-3-yl]-2-methyl-propanoic Acid 3-Cyano-propyl Ester (10a)—

The synthesis was carried out as described for **7a** using **9b** (110 mg, 0.24 mmol) and sodium cyanide (118 mg, 2.4 mmol) in anhydrous DMSO and gave **10a** (95 mg, 98% yield) as light-yellow gum. IR ($CHCl_3$): 3403, 2971, 2248 (CN), 1727 and 1704 (s, $>C=O$), 1621, 1576, 1421, 1261, 1185 cm^{-1} . 1H NMR (500 MHz, $CDCl_3$) δ 6.40 (d, $J = 2.0$ Hz, 1H, 4-H), 6.29 (d, $J = 2.0$ Hz, 1H, 2-H), 5.82 (s, 1H, OH), 5.42 (m as d, $J = 4.0$ Hz, 1H, 8-H), 4.17 (m, AB system, 2H, $-OCH_2-$), 3.22 (dd, $J = 15.0$ Hz, $J = 4.5$ Hz, 1H, 10α -H), 2.70 (td, $J = 11.0$ Hz, $J = 4.5$ Hz, 1H, $10a$ -H), 2.21 (t, $J = 7.5$ Hz, 2H, $-CH_2CN$), 2.18–2.10 (m, 1H, 7α -H), 1.93 (m as qt, $J = 6.0$ Hz, 2H, $-CH_2-$ of the side chain), 1.87–1.75 (m, 3H, 10β -H, 7β -H, $6a$ -H), 1.70 (s, 3H, 9- CH_3), 1.52 (s, 6H, $-C(CH_3)_2-$), 1.38 (s, 3H, 6β - CH_3), 1.10 (s, 3H, 6α - CH_3). Mass spectrum (EI) m/z (relative intensity) 397 (M^+ , 79), 382 (12), 354 (9), 329 (13), 314 (100), 285 (27), 276 (21), 241 (78), 149 (21), 70 (41). Exact mass (EI) calculated for $C_{24}H_{31}NO_4$ (M^+), 397.2253; found, 397.2254. LC/MS analysis (Waters MicroMass ZQ system) showed purity 98% and retention time 11.4 min for the title compound. Anal. ($C_{24}H_{31}NO_4$) C, H, N.

2-[(6aR,10aR)-6a,7,10,10a-Tetrahydro-1-hydroxy-6,6,9-trimethyl-6H-dibenzo[b,d]pyran-3-yl]-2-methyl-propanoic Acid 3-(1H-Imidazol-1-yl)propyl Ester (10b)—

To a stirred suspension of **9b** (196.0 mg, 0.43 mmol) and potassium carbonate (594 mg, 4.30 mmol) in DMSO (5 mL) was added imidazole (146 mg, 2.15 mmol) at room temperature under an argon atmosphere. Stirring was continued for 14 h, and then the mixture was diluted with water and ethyl acetate. The organic layer was separated, and the aqueous layer was extracted with ethyl acetate. The combined organic layer was washed with water and brine, dried ($MgSO_4$), and concentrated in vacuo. Purification by flash column chromatography on silica gel (50% acetone in hexane) gave **10b** (78 mg, 41% yield) as light-yellow gum. IR ($CHCl_3$): 2971, 2932, 1727 (s, $>C=O$), 1618, 1578, 1512, 1417, 1251 cm^{-1} . 1H NMR (500 MHz, $CDCl_3$) δ 7.33 (s, 1H, imidazole), 7.04 (s, 1H, imidazole), 6.44 (s, 1H, imidazole), 6.40 (d, $J = 2.0$ Hz, 1H, 4-H), 6.32 (d, $J = 2.0$ Hz, 1H, 2-H), 5.40 (m as d, $J = 5.0$ Hz, 1H, 8-H), 3.93 (td, $J = 17.0$ Hz, $J = 5.5$ Hz, 1H, $-OCH_2-$), 3.85 (td, $J = 17.0$ Hz, $J = 5.5$ Hz, 1H, $-OCH_2-$), 3.72 (t, $J = 7.0$ Hz, 2H, $-CH_2-N<$), 3.41 (dd, $J = 16.0$ Hz, $J = 4.5$ Hz, 1H, 10α -H), 2.73 (td, $J = 11.0$ Hz, $J = 4.5$ Hz, 1H, $10a$ -H), 2.17–2.09 (m, 1H, 7α -H), 2.01–1.93 (m, 2H, $-OCH_2-CH_2-$), 1.85–1.71 (m, 3H, 10β -H, 7β -H, $6a$ -H), 1.60 (s, 3H, 9- CH_3), 1.50 (s, 3H, $-C(CH_3)_2-$), 1.49 (s, 3H, $-C(CH_3)_2-$), 1.38 (s, 3H, 6β - CH_3), 1.08 (s, 3H, 6α - CH_3). ^{13}C NMR (100 MHz, $CDCl_3$) δ 176.8 ($>C=O$), 157.4 (C-1 or C-5), 155.1 (C-5 or C-1), 143.8, 137.5 (imidazole), 135.4, 128.7 (imidazole), 119.4, 119.2, 112.6, 106.0 (C-2 or C-4), 105.7 (C-4 or C-2), 77.0 (C-6), 60.9 ($-OCH_2-$), 46.2, 45.2, 43.8, 36.0, 31.9, 29.8, 28.1, 27.8, 26.1, 25.8, 23.7, 18.7. Mass spectrum (EI) m/z (relative intensity) 438 (M^+ , 62), 423 (12), 395 (80, 355 (7), 317 (6), 304 (10), 285 (7), 201 (6), 149 (10, 88 (18), 56 (100). Exact mass (EI) calculated for $C_{26}H_{34}N_2O_4$ (M^+), 438.2519; found, 438.2518. HPLC (4.6 mm \times 250 mm, Supelco discovery column, acetonitrile/water) showed purity 98% and retention time 7 min for the title compound. LC/MS analysis (Waters

MicroMass ZQ system) showed purity 98% and retention time 5.5 min for the title compound.

2-(3,5-Dimethoxyphenyl)-2-methylpropanal³⁴ (12)—To a solution of **11** (3.0 g, 14.6 mmol) in dry CH₂Cl₂ (50 mL) at -78 °C under an argon atmosphere was added dropwise DIBAL-H (37 mL, 37 mmol, 1 M solution in CH₂Cl₂). The reaction mixture was stirred at the same temperature for 1 h and then quenched by dropwise addition of potassium sodium tartrate (10% solution in water). The resulting mixture was warmed to room temperature, stirred vigorously for 40 min, and then diluted with ethyl acetate. The organic phase was separated, and the aqueous phase was extracted with ethyl acetate. The combined organic layer was washed with brine, dried (MgSO₄), and concentrated under reduced pressure. Purification by flash column chromatography on silica gel (20% ethyl acetate in hexane) gave **12** (2.8 g, 94%) as a colorless oil. IR (neat): 2970, 2937, 1725 (s, >C=O), 1592, 1456, 1423, 1204, 1159, 1048 cm⁻¹. ¹H NMR (500 MHz, CDCl₃) δ 9.46 (s, -CH=O), 6.40 (d, *J* = 2.0 Hz, 2H, ArH), 6.39 (t, *J* = 2.0 Hz, 1H, ArH), 3.79 (s, 6H, -OCH₃), 1.43 (s, 6H, -C(CH₃)₂-). Mass spectrum (EI) *m/z* (relative intensity) 208 (M⁺, 25), 196 (16), 179 (M⁺ - CHO), 165 (25), 151 (14), 139 (39), 91 (20), 77 (20). Exact mass (EI) calculated for C₁₂H₁₆O₃ (M⁺), 208.1099; found, 208.1108.

2-(3,5-Dimethoxyphenyl)-2-methylpropan-1-ol (13)—To a solution of **12** (1.70 g, 8.16 mmol) in anhydrous methanol (40 mL) at room temperature under an argon atmosphere was added sodium borohydride (1.39 g, 36.7 mmol) portionwise. The reaction mixture was stirred for 1 h and then quenched by the addition of aqueous 1 N HCl and extracted with ethyl acetate. The organic layer was washed with brine, dried (MgSO₄), and evaporated. Purification by flash column chromatograph on silica gel (20% ethyl acetate in hexane) gave **13** (1.6 g, 94%) as a colorless oil. IR (neat): 3433 (br, OH), 2961, 2836, 1592, 1456, 1422, 1202, 1159, 1048 cm⁻¹. ¹H NMR (500 MHz, CDCl₃) δ 6.53 (d, *J* = 2.0 Hz, 2H, ArH), 6.34 (t, *J* = 2.0 Hz, 1H, ArH), 3.80 (s, 6H, -OCH₃), 3.58 (s, 2H, -CH₂OH), 1.30 (s, 6H, -C(CH₃)₂-). Mass spectrum (ESI) *m/z* (relative intensity) 211 (M⁺ + H, 100).

5-(1-Hydroxy-2-methylpropan-2-yl)resorcinol (14)—To a stirred solution of **13** (400 mg, 1.9 mmol) in dry CH₂Cl₂ (20 mL) at -78 °C, under an argon atmosphere, was added boron tribromide (6.6 mL, 6.6 mmol, 1 M solution in CH₂Cl₂). Following this addition, the reaction temperature was gradually raised over a period of 3 h to 25 °C, and the stirring was continued at that temperature until the reaction was completed (4 h). Unreacted boron tribromide was destroyed by the addition of methanol and ice at 0 °C. The resulting mixture was warmed to room temperature, and volatiles were removed in vacuo. The residue was dissolved in diethyl ether and washed with water and brine and dried (MgSO₄). Solvent evaporation and purification by flash column chromatography on silica gel (40% diethyl ether in hexane) gave **14** (165 mg, 47%) as light-yellow oil. IR (neat): 3443 (br, OH), 2959, 1591, 1458, 1420, 1201, 1048 cm⁻¹. ¹H NMR (500 MHz, CDCl₃) δ 6.43 (d, *J* = 2.0 Hz, 2H, ArH), 6.22 (t, *J* = 2.0 Hz, 1H, ArH), 4.84 (s, 2H, ArOH), 3.56 (d, *J* = 6.0 Hz, 2H, -CH₂OH), 1.28 (s, 6H, -C(CH₃)₂-). Mass spectrum (ESI) *m/z* (relative intensity) 183 (M⁺ + H, 35), 165 (100).

(6aR,10aR)-3-(1-Hydroxy-2-methylpropan-2-yl)-6a,7,10,10a-tetrahydro-6,6,9-trimethyl-6H-dibenzo[b,d]pyran-1-ol (15)—To a stirred solution of **14** (165 mg, 0.9 mmol) and (+)-*cis/trans*-*p*-mentha-2,8-dien-1-ol (166 mg, 1.09 mmol) in anhydrous CHCl₃ (3 mL), under an argon atmosphere, was added *p*-toluenesulfonic acid (52 mg, 0.3 mmol). The reaction mixture was heated at 150 °C for 10 min using microwave irradiation, and then it was cooled to room temperature and diluted with water and CHCl₃. The organic layer was separated, and the aqueous phase was extracted with CHCl₃. The combined organic layer was washed with water and brine and dried (MgSO₄). Solvent evaporation and purification by flash column chromatography on silica gel (15% ethyl acetate in hexane) gave **15** (80 mg, 28%) as an orange solid, mp 91–93 °C. IR (CHCl₃): 3341 (br, OH), 2968, 1621, 1575, 1415, 1329, 1185 cm⁻¹. ¹H NMR (500 MHz, CDCl₃) δ 6.42 (d, *J* = 1.5 Hz, 1H, 4-H), 6.28 (d, *J* = 1.5 Hz, 1H, 2-H), 5.43 (m as d, *J* = 4.5 Hz, 1H, 8-H), 3.54 (s, 2H, –CH₂OH), 3.22 (dd, *J* = 15.5 Hz, *J* = 4.5 Hz, 1H, 10 α -H), 2.70 (td, *J* = 11.0 Hz, *J* = 4.5 Hz, 1H, 10 α -H), 2.19–2.11 (m, 1H, 7 α -H), 1.90–1.71 (m, 3H, 10 β -H, 7 β -H, 6 α -H), 1.70 (s, 3H, 9-CH₃), 1.38 (s, 3H, 6 β -CH₃), 1.24 (s, 6H, –C(CH₃)₂–), 1.08 (s, 3H, 6 α -CH₃). Mass spectrum (ESI) *m/z* (relative intensity) 317 (M⁺ + H, 100). LC/MS analysis (Waters MicroMass ZQ system) showed purity 97% and retention time 5.7 min for the title compound.

2-[(6aR,10aR)-6a,7,10,10a-Tetrahydro-1-hydroxy-6,6,9-trimethyl-6H-dibenzo[b,d]pyran-3-yl]-2-methyl propylpentanoate (16)—To a stirred solution of **15** (180 mg, 0.57 mmol), valeric acid (1.0 mL, 0.8 mmol) and triphenylphosphine (223 mg, 0.85 mmol) in anhydrous THF (10 mL) at 0 °C, under an argon atmosphere, was added diethyl azodicarboxylate (0.15 mL, 0.8 mmol) dropwise. The reaction temperature was raised to 25 °C, and stirring was continued for 20 h. The reaction mixture was quenched with aqueous 1 N HCl solution and extracted with ethyl acetate. The organic phase was washed with water and brine and dried (MgSO₄). Solvent evaporation and purification by flash column chromatography on silica gel (25% ethyl acetate in hexane) gave **16** (93 mg, 41%) as light-yellow gum. IR (CHCl₃): 3389 (br, OH), 2968, 2891, 1710 (>C=O), 1620, 1578, 1417, 1332, 1186 cm⁻¹. ¹H NMR (500 MHz, CDCl₃) δ 6.42 (d, *J* = 2.0 Hz, 1H, 4-H), 6.26 (d, *J* = 2.0 Hz, 1H, 2-H), 5.43 (m as d, *J* = 5.0 Hz, 1H, 8-H), 4.94 (s, 1H, OH), 4.05 (s, 2H, –CH₂O–), 3.19 (dd, *J* = 15.5 Hz, *J* = 5.5 Hz, 1H, 10 α -H), 2.69 (td, *J* = 11.0 Hz, *J* = 4.5 Hz, 1H, 10 α -H), 2.28 (t, *J* = 7.0 Hz, 2H, –CH₂-C(O)–), 2.19–2.11 (m, 1H, 7 α -H), 1.89–1.74 (m, 3H, 10 β -H, 7 β -H, 6 α -H), 1.70 (s, 3H, 9-CH₃), 1.55 (qt, *J* = 7.0 Hz, 2H, –CH₂– of the side chain), 1.38 (s, 3H, 6 β -CH₃), 1.32–1.24 (m and s overlapping, 8H, –C(CH₃)₂– and –CH₂– of the side chain, especially 1.28, s, –C(CH₃)₂–), 1.10 (s, 3H, 6 α -CH₃), 0.88 (t, *J* = 7.0 Hz, 3H, –CH₂-CH₃). Mass spectrum (EI) *m/z* (relative intensity) 400 (M⁺, 100), 385 (9), 357 (11), 327 (35), 317 (27), 285 (26), 255 (17), 217 (9). Exact mass (EI) calculated for C₂₅H₃₆O₄ (M⁺), 400.2614; found, 400.2611. Anal. (C₂₅H₃₆O₄) C, H.

2-[(6aR,10aR)-6a,7,10,10a-Tetrahydro-1-hydroxy-6,6,9-trimethyl-6H-dibenzo[b,d]pyran-3-yl]-2-methyl-N-pentylpropanamide (18)—Carboxylic acid intermediate **5b** (200 mg, 0.61 mmol) was dissolved in dry CH₂Cl₂ (3 mL) under an argon atmosphere and cooled to 0 °C. To the cold solution, triethylamine (0.12 mL, 0.92 mmol) was added followed by the dropwise addition of bis(2-methoxyethyl)aminosulfur trifluoride (0.13 mL, 0.72 mmol). After stirring for 15 min, a solution of amylamine (80 mg, 0.92

mmol) in dry CH_2Cl_2 (6 mL) was added. The resulting mixture was stirred at 0 °C for 15 min and at 25 °C for 2 h and then diluted with CH_2Cl_2 and saturated aqueous sodium bicarbonate solution. The organic layer was separated, and the aqueous layer was extracted with ethyl acetate. The combined organic layer was washed with water and brine, dried (MgSO_4), and concentrated in vacuo. Purification by flash column chromatography on silica gel (12% ethyl acetate in hexane) afforded **18** (170 mg, 70% yield) as light-yellow gum. IR (neat): 3274, 2930, 1643, and 1618 ($>\text{C}=\text{O}$), 1577, 1518, 1415, 1264, 1183, 1083 cm^{-1} . ^1H NMR (500 MHz, CDCl_3) δ 8.53 (s, 1H, $>\text{NH}$), 6.40 (d, $J = 1.5$ Hz, 1H, 4-H), 6.25 (d, $J = 1.5$ Hz, 1H, 2-H), 5.46–5.35 (m as d, $J = 5.0$ Hz, and br s overlapping, 2H, 8-H, OH), 3.41 (dd, $J = 16.0$ Hz, $J = 4.5$ Hz, 1H, 10 α -H), 3.12 (m as q, $J = 7.0$ Hz, 2H, $-\text{CH}_2-\text{N}<$), 2.73 (td, $J = 11.0$ Hz, $J = 4.5$ Hz, 1H, 10 α -H), 2.20–2.15 (m, 1H, 7 α -H), 1.88–1.76 (m, 3H, 10 β -H, 7 β -H, 6 α -H), 1.70 (s, 3H, 9- CH_3), 1.49 (s, 6H, $-\text{C}(\text{CH}_3)_2-$), 1.40 (s, 3H, 6 β - CH_3), 1.36 (qt, $J = 7.0$ Hz, 2H, $-\text{CH}_2-$ of the side chain), 1.18 (qt, $J = 7.0$ Hz, 2H, $-\text{CH}_2-$ of the side chain), 1.16–1.08 (m and s overlapping, 5H, 6 α - CH_3 , $-\text{CH}_2-$ of the side chain, especially 1.14, s, 6 α - CH_3), 0.81 (t, $J = 7.0$ Hz, 3H, $-\text{CH}_2-\text{CH}_3$). Mass spectrum (EI) m/z (relative intensity) 399 (M^+ , 25), 286 (100), 220 (21), 205 (82), 164 (15), 149 (18), 88 (23). Exact mass (EI) calculated for $\text{C}_{25}\text{H}_{37}\text{NO}_3$ (M^+), 399.2773; found, 399.2777. LC/MS analysis (Waters MicroMass ZQ system) showed purity 96% and retention time 5.7 min for the title compound.

2-[(6aR,10aR)-6a,7,10,10a-Tetrahydro-1-hydroxy-6,6,9-trimethyl-6H-dibenzo[b,d]pyran-3-yl]-2-methyl-propanoyl Chloride (19)—

To a stirred solution of acid **5b** (90 mg, 0.27 mmol) in dry CH_2Cl_2 (3.4 mL), at room temperature under an argon atmosphere, was added the SOCl_2 –BTA reagent (0.23 mL (0.35 mmol) of a 1.5 M solution in CH_2Cl_2 , which was prepared by dissolving 0.54 mL (7.5 mmol) of SOCl_2 and 0.893 g (7.5 mmol) of BTA in 5 mL CH_2Cl_2). Stirring was continued for 20 min, and insoluble materials were filtered off. The filtrate was washed with aqueous 1 N HCl, water, and brine, and then dried (MgSO_4). Solvent evaporation under reduced pressure afforded the title compound (95 mg) which was used in the next step without further purification.

S-Propyl-2-[(6aR,10aR)-6a,7,10,10a-tetrahydro-1-hydroxy-6,6,9-trimethyl-6H-dibenzo[b,d]pyran-3-yl]-2-methylpropanethioate (20)—

To a solution of **19** (95 mg, 0.27 mmol) and propanethiol (54 mg, 64 μL , 0.71 mmol) in dry CH_2Cl_2 (5.4 mL) at room temperature, under an argon atmosphere, was added anhydrous pyridine (0.3 mL). The reaction mixture was stirred for 3 h and then diluted with water and diethyl ether. The organic layer was separated, and the aqueous layer was extracted with diethyl ether. The combined organic layer was washed with water and brine, dried (MgSO_4), and concentrated in vacuo. Purification by flash column chromatography on silica gel (5–15% diethyl ether in hexane) gave **20** (24 mg, 23% yield for the two steps) as a pale-yellow gum. IR (CHCl_3): 3435, 2966, 2927, 1678, and 1652 (s, $>\text{C}=\text{O}$), 1620, 1579, 1417, 1264 cm^{-1} . ^1H NMR (500 MHz, CDCl_3) δ 6.45 (d, $J = 2.0$ Hz, 1H, 4-H), 6.24 (d, $J = 2.0$ Hz, 1H, 2-H), 5.42 (m as d, $J = 5.0$ Hz, 1H, 8-H), 5.02 (br s, 1H, OH), 3.19 (dd, $J = 16.0$ Hz, $J = 4.5$ Hz, 1H, 10 α -H), 2.78 (m as t, $J = 7.5$ Hz, 1H, $-\text{SCH}_2-$), 2.77 (m as t, $J = 7.5$ Hz, 1H, $-\text{SCH}_2-$), 2.70 (td, $J = 11.0$ Hz, $J = 4.5$ Hz, 1H, 10 α -H), 2.18–2.10 (m, 1H, 7 α -H), 1.90–1.74 (m, 3H, 10 β -H, 7 β -H, 6 α -H), 1.70 (s, 3H, 9- CH_3), 1.58–1.50 (m and s overlapping, 8H, $-\text{C}(\text{CH}_3)_2-$, $-\text{CH}_2-$ of the side

chain, especially 1.54, s, $-\text{C}(\text{CH}_3)_2-$, 1.38 (s, 3H, $6\beta\text{-CH}_3$), 1.09 (s, 3H, $6\alpha\text{-CH}_3$), 0.92 (t, $J = 7.5$ Hz, 3H, $-\text{CH}_2\text{-CH}_3$). Mass spectrum (EI) m/z (relative intensity) 388 (M^+ , 19), 285 (100). Exact mass (EI) calculated for $\text{C}_{23}\text{H}_{32}\text{O}_3\text{S}$ (M^+), 388.2072; found, 388.2075. LC/MS analysis (Waters MicroMass ZQ system) showed purity 98% and retention time 7.8 min for the title compound.

Radioligand Binding Assays

Rat brain CB1 receptor, mouse and human CB2 receptor binding assays: Compounds were tested for their affinities for the CB1 and CB2 receptors using membrane preparations from rat brain or HEK293 cells expressing either mCB2 or hCB2 receptors, respectively, and [^3H]CP-55,940, as previously described.^{18,20,32} Results from the competition assays were analyzed using nonlinear regression to determine the IC_{50}^{35} values for the ligand; K_i values were calculated from the IC_{50} (Prism by GraphPad Software, Inc.). Each experiment was performed in triplicate, and K_i values determined from three independent experiments and are expressed as the mean of the three values.

cAMP Assay.^{16,18}

HEK293 cells stably expressing rCB1 receptor were used for the studies. The cAMP assay was carried out using PerkinElmer's Lance ultra cAMP kit following the protocol of the manufacturer. Briefly, the assays were carried out in 384-well plates using 1000–1500 cells/well. The cells were harvested with non-enzymatic cell dissociation reagent Versene and were washed once with HBSS and resuspended in the stimulation buffer. The various concentrations of the test compound (5 μL) in forskolin (2 μM final concentration) containing stimulation buffer were added to the plate followed by the cell suspension (5 μL). The cells were stimulated for 30 min at room temperature. Then Eu-cAMP tracer working solution (5 μL) and Ulight-anti-cAMP working solution (5 μL) were added to the plate and incubated at room temperature for 60 min. The data were collected on a PerkinElmer Envision instrument. The EC_{50} values were determined by nonlinear regression analysis using GraphPad Prism software (GraphPad Software, Inc., San Diego, CA).

Plasma Stability.^{16,36}

Compounds or their proposed products were diluted (200 μM) in mouse plasma and incubated at 37 °C, 100 rpm. At various time points, samples were taken, diluted 1:4 in acetonitrile, and centrifuged to precipitate the proteins. The resulting supernatant was analyzed by HPLC. In vitro plasma half-lives were determined using exponential decay calculations in Prism (GraphPad).

HPLC Analysis—Chromatographic separation was achieved using a Supelco Discovery C18 (4.6 mm \times 250 mm) column on a Waters Alliance HPLC system. Mobile phase consisted of acetonitrile (A) and a mixture of 60% water (acidified with 8.5% *o*-phosphoric acid) and 40% acetonitrile (B). Gradient elution started with 5% A, transitioning to 95% A over 10 min and holding for 5 min before returning to starting conditions; run time was 15 min, the flow rate was 1 mL/min, and UV detection was used at each compound's maximal absorbance (204 and 230 nm).

Molecular Modeling

Ballesteros–Weinstein Nomenclature—The Ballesteros–Weinstein numbering system for GPCR amino acid residues is used here.³⁷ In this numbering system, the label 0.50 is assigned to the most highly conserved class A residue in each trans-membrane helix (TMH). This is preceded by the TMH number. In this system, for example, the most highly conserved residue in TMH6 is P6.50. The residue immediately before this would be labeled 6.49, and the residue immediately after this would be labeled 6.51. When referring to a specific CB1 residue, the Ballesteros–Weinstein name is followed by the absolute sequence number given in parentheses (e.g., K3.28(192)); however, when referring to a highly conserved residue among class A GPCRs (and not a specific residue in CB1), only the Ballesteros–Weinstein name is given.

Conformational Searches—The structures of the ligands (-)- δ -THC, (-)- δ -THC-dimethylheptyl, and **10a** were built in Spartan'08 (Wave function, Inc., Irvine, CA). Initial conformational analyses of these compounds were performed in vacuo using the semiempirical method RM1 encoded in Spartan'08. Conformational searches were performed (using 3–8-fold rotations) for each rotatable bond. All unique conformers identified were then optimized with ab initio Hartree–Fock calculations at the 6–31G* level. To calculate the difference in energy between the global minimum energy conformer of each compound and its final docked conformation, rotatable bonds in the global minimum energy conformer were driven to their corresponding value in the final docked conformation and the single-point energy of the resultant structure was calculated at the HF 6–31G*. A duplicate conformational search of **10a** was conducted at high dielectric using the MCMM (Monte Carlo multiple minimum) protocol in MacroModel with the OPLS_2005 force field in a GB/SA water model with an extended cutoff.^{38,39} An energy window of 21.0 kJ/mol (5 kcal/mol) was employed, and the redundant conformers of **10a** were eliminated using a rmsd cutoff of 0.5 Å for all atoms.

CB1R Active State Model—The studies reported here used our previously published CB1 activated state model.⁴⁰ Below, we describe briefly the construction of both the inactive and active states of this model. Because no crystal structure of the CB1 receptor has been published, the CB1 model uses the crystal structure of the class A GPCR rhodopsin in the dark state as its template.⁴¹ This template was chosen because no mutations or modifications were made to its structure for crystallization and because the cannabinoid receptors and rhodopsin share some unusual sequence motifs that have important spatial relevance. For example, these receptors share a TMH4 GWNC motif at their extracellular ends. Here a TRP forms an aromatic stacking interaction with Y5.39, influencing the extracellular (EC) positions of TMH3–4–5. Changes to the general Rho structure that were necessitated by sequence divergences included the absence of helix kinking proline residues in TMH1 and TMH5, the lack of a GG motif in TMH2 (at position 2.56 and 2.57), as well as the presence of extra flexibility in the TMH6 CWXP motif because of the presence of G6.49 immediately before P6.50.⁴² An activated state (R*) CB1 model was created by modification of our inactive state model. This R* model construction was guided by the biophysical literature on the R-to-R* transition in rhodopsin (Rho) and included a TMH6 conformer derived from our Conformational Memories study of CB1 TMH6 that is

straightened, breaking the ionic lock interaction between R3.50 and D6.30.⁴³ Extracellular (EC-1, H181–S185; EC-2, C257–E273; EC-3, D366–K376) and intracellular (IC-1, S146–R150; IC-2, P221–V228; IC-3, A301–P332) loops, as well as portions of the N (K90–N112) and C termini (S414–G427), were then added to the refined model of the CB1 R* bundle. The Modeler program was then used to refine loop structures.^{44,45} Specific conformations of the EC-2 and EC-3 loop were refined to reflect mutagenesis data showing that EC-2 loop residue F(268) should be available to the binding crevice and that EC-3 loop residue K(373) should interact in a salt bridge with TMH2 residue D2.63(176).^{46,47}

Ligand/CB1R* Complexes—The automatic docking program, Glide v6.4 (Schrödinger, LLC, NY 2014) was used to explore possible binding conformations or receptor site interactions for subject ligands. Because K3.28(192) has been shown to be a critical residue for classical cannabinoid binding,⁴⁸ K3.28(192) was defined as a required interaction during the docking procedure. Glide was used to generate a grid based on the centroid of the ligand in the binding site. Any hydrophobic region defined in the grid generation that contacted the ligand was selected as important to the docking procedure. The box for Glide docking was defined to be 22 Å in the *x*, *y*, and *z* dimensions. The lowest energy conformations (<4 kcal/mol above the global min) of each ligand were docked using Glide. Extra precision (XP) was selected with no scaling of VdW radii and rigid docking invoked. Glide scoring functions do not take into account the conformational cost, or internal strain energy, of each generated pose of a ligand inside the binding pocket of the receptor. To determine the best ligand/receptor complex to proceed with a postdocking minimization for the acquisition of pairwise interaction energies, the conformational cost for each pose was subtracted from the Glide score for all poses (Supporting Information, Tables S2–4). The pose with the final best score was then subjected to a post docking minimization in two stages using the OPLS2005 all atom force field in Macromodel 10.5 (Schrödinger, LLC, NY 2014). An 8.0 Å nonbonded cutoff (updated every 10 steps), a 20.0 Å electrostatic cutoff, and a 4.0 Å hydrogen bond cutoff were used in each stage of the calculation. The first stage consisted of Polak–Ribier conjugate gradient minimization using a distance-dependent dielectric function with a base constant of 2. No harmonic constraints were placed on the side chains, but 1000 kJ/mol fixed atom constraints were applied to hold all the backbone atoms in place. The termini and loops were not allowed to move during this part of the procedure. The minimization was continued until the bundle reached the 0.05 kJ/mol·Å² gradient. To relax the loops, a second stage Polak–Ribier conjugate gradient minimization of the loop regions was performed until the 0.05 kJ/mol·Å² gradient was reached. The loop and termini regions were left free, while the transmembrane regions and ligand were not allowed to move during this final stage. An 8.0 Å extended nonbonded cutoff (updated every 10 steps), 20.0 Å electrostatic cutoff, and 4.0 Å hydrogen bond cutoff were used in this calculation, and the generalized Born/surface area (GB/SA) continuum solvation model for water available in Macromodel was employed.

Assessment of Pairwise Interaction and Total Energies—Interaction energies between each bound ligand and residue in the CB1R* complex were calculated using Macromodel, as described previously.⁴⁹ Specifically, after defining the atoms of the ligand as one group (group 1) and the atoms corresponding to a residue that lines the binding site in

the final ligand-CB1R* complex as another group (group 2), Macromodel was used to output the pairwise interaction energy (Coulombic and van der Waals) for a given pair.

Methods for Characterization of in Vivo Effects.^{18,50}

Subjects—For hypothermia testing, female Sprague–Dawley rats ($n = 6/\text{group}$), weighing between 250 and 350 g (Charles River, Wilmington MA) were used. Rats were tested repeatedly with at least 5 days intervening between drug sessions. Experiments occurred at approximately the same time (10:00 a.m.–5:00 p.m.) during the light portion of the daily light/dark cycle. Outside of experimental sessions, rats were pair housed (2/cage) in a climate controlled vivarium with unrestricted access to food and water. For tail-flick withdrawal (analgesia) testing, male CD-1 mice ($n = 6/\text{group}$), weighing between 30 and 35 g (Charles River, Wilmington MA), were used. Mice were housed 4/cage in a climate controlled vivarium with unrestricted access to food and water and acclimated to these conditions for at least a week before any experimental manipulations occurred. Analgesia testing took place between 11:00 a.m. and 7:00 p.m. Mice were used once.

Procedures—Temperature was recorded using a thermistor probe (Model 401, Measurement Specialties, Inc., Dayton, OH) inserted to a depth of 6 cm and secured to the tail with micropore tape. Rats were minimally restrained and isolated in $38 \times 50 \times 10 \text{ cm}^3$ plastic stalls. Temperature was read to the nearest 0.01 °C using a thermometer (model 4000A, Measurement Specialties, Inc.).

Two baseline temperature measures were recorded at 15 min intervals, and drugs were injected immediately after the second baseline was recorded. After injection, temperature was recorded every 30 min for 3 h and every hour thereafter for a total of 6 h. In some studies, temperature readings at later time points were obtained by inserting the probe 6 cm and holding it in place for at least 1 min before taking a reading. The change in temperature was determined for each rat by subtracting temperature readings from the average of the two baseline measures. Analgesia testing utilized a thermostatically controlled 2 L water bath commercially available from VWR International where the water temperature was set at 52 °C (± 0.5 °C). The tail was immersed into the water at a depth of 2 cm and the withdrawal latency recorded by a commercially available stopwatch (Fisher Scientific), allowing measurements in seconds and 1/100 s. Cut-off was set at 10 s to minimize the risk of tissue damage. A test session consisted of five recordings, the first of which constituted the baseline recording. Injections occurred immediately after the baseline recording, and the remaining recordings took place 20, 60, 180, and 360 min post administration. Prior to this testing, the animals had been accustomed to the procedure for three consecutive “mock” sessions where the water was held at 38 °C, i.e., average body temperature of mice; no tail-flicks were elicited by this water temperature. The third “mock” session also included an ip injection of vehicle (10 mL/kg). The tail-flick withdrawal latencies are expressed as a percentage of maximum possible effect (%MPE), according to the formula:
$$\%MPE = [(\text{test latency} - \text{baseline latency}) / (10 - \text{baseline latency})] \times 100.$$

Drugs—For hypothermia testing, (–)-⁸-THC-DMH and compounds **2b** and **10a** were initially dissolved in a solution of 20% ethanol, 20% alkamuls, and 60% saline and were

further diluted with saline. Injections were administered sc in a volume of 1.0 mL/kg. For tail-flick withdrawal (analgesia) testing, **10a** and **2b** were initially dissolved in 2% dimethyl sulfoxide, 4% Tween-80, and 4% propylene glycol before saline was slowly added just prior to the 10 mL/kg ip administration. All suspensions were freshly prepared for analgesia testing.

Data Analysis—Time-effect functions for hypothermia testing were analyzed using two-way repeated measures ANOVA procedures followed by Bonferroni's posthoc test. Hypothermia dose-effect functions for compounds (–)-⁸-THC-DMH, **2b**, and **10a** were analyzed using one-way repeated measures ANOVA procedures followed by the Holm–Sidak multiple comparison *t*-test; *p* was set at 0.05, and statistical analyses were performed using the software package GraphPad Prism 5.03 (GraphPad Software, San Diego, CA). A linear mixed model repeated measures ANOVA (IBM software package SPSS, v.21) was applied to tail-flick latency data depicted in Figure 5.

Supplementary Material

Refer to Web version on PubMed Central for supplementary material.

Acknowledgments

This work was supported by grants from the National Institute on Drug Abuse to A.M., DA009158, DA007215, and DA09064.

ABBREVIATIONS USED

CB1	cannabinoid receptor 1
CB2	cannabinoid receptor 2
(–)- ⁹ - THC	(–)- ⁹ -tetrahydrocannabinol
CNS	central nervous system
PK/PD	pharmacokinetic/pharmacodynamic
SC	side chain
SAR	structure–activity relationship
HEK293	human embryonic kidney cell line
log <i>P</i>	octanol–water partition coefficient
PSA	polar surface area
NMR	nuclear magnetic resonance
HPLC	high-performance liquid chromatography

References

1. Mechoulam R, Hanus L. A historical overview of chemical research on cannabinoids. *Chem Phys Lipids*. 2000; 108:1–13. [PubMed: 11106779]

2. Devane WA, Dysarz FA III, Johnson MR, Melvin LS, Howlett AC. Determination and characterization of a cannabinoid receptor in rat brain. *Mol Pharmacol*. 1988; 34:605–613. [PubMed: 2848184]
3. Munro S, Thomas KL, Abu-Shaar M. Molecular characterization of a peripheral receptor for cannabinoids. *Nature*. 1993; 365:61–65. [PubMed: 7689702]
4. Pavlopoulos S, Thakur GA, Nikas SP, Makriyannis A. Cannabinoid receptors as therapeutic targets. *Curr Pharm Des*. 2006; 12:1751–1769. [PubMed: 16712486]
5. Buchwald A, Derendorf H, Ji F, Nagaraja NY, Wu WM, Bodor N. Soft cannabinoid analogues as potential anti-glaucoma agents. *Pharmazie*. 2002; 57:108–114. [PubMed: 11878185]
6. Hwang J, Adamson C, Butler D, Janero DR, Makriyannis A, Bahr BA. Enhancement of endocannabinoid signaling by fatty acid amide hydrolase inhibition: a neuroprotective therapeutic modality. *Life Sci*. 2010; 86:615–623. [PubMed: 19527737]
7. Jarvinen T, Pate DW, Laine K. Cannabinoids in the treatment of glaucoma. *Pharmacol Ther*. 2002; 95:203–220. [PubMed: 12182967]
8. Karst M, Wippermann S, Ahrens J. Role of cannabinoids in the treatment of pain and (painful) spasticity. *Drugs*. 2010; 70:2409–2438. [PubMed: 21142261]
9. Lu D, Vemuri VK, Duclos RI Jr, Makriyannis A. The cannabinergic system as a target for anti-inflammatory therapies. *Curr Top Med Chem*. 2006; 6:1401–1426. [PubMed: 16918457]
10. Marco EM, Romero-Zerbo SY, Viveros MP, Bermudez-Silva FJ. The role of the endocannabinoid system in eating disorders: pharmacological implications. *Behav Pharmacol*. 2012; 23:526–536. [PubMed: 22785439]
11. Pacher P, Batkai S, Kunos G. The endocannabinoid system as an emerging target of pharmacotherapy. *Pharmacol Rev*. 2006; 58:389–462. [PubMed: 16968947]
12. Pertwee RG. Cannabinoid receptors and pain. *Prog Neurobiol*. 2001; 63:569–611. [PubMed: 11164622]
13. Pertwee RG. The diverse CB1 and CB2 receptor pharmacology of three plant cannabinoids: delta9-tetrahydrocannabinol, cannabidiol and delta9-tetrahydrocannabivarin. *Br J Pharmacol*. 2008; 153:199–215. [PubMed: 17828291]
14. Han S, Thatte J, Buzard DJ, Jones RM. Therapeutic utility of cannabinoid receptor type 2 (CB2) selective agonists. *J Med Chem*. 2013; 56:8224–8256. [PubMed: 23865723]
15. Grotenhermen F. Pharmacokinetics and pharmacodynamics of cannabinoids. *Clin Pharmacokinet*. 2003; 42:327–360. [PubMed: 12648025]
16. Sharma R, Nikas SP, Paronis CA, Wood JT, Halikhedkar A, Guo JJ, Thakur GA, Kulkarni S, Benchama O, Raghav JG, Gifford RS, Jarbe TU, Bergman J, Makriyannis A. Controlled-deactivation cannabinergic ligands. *J Med Chem*. 2013; 56:10142–10157. [PubMed: 24286207]
17. Sharma R, Nikas SP, Guo JJ, Mallipeddi S, Wood JT, Makriyannis A. C-Ring cannabinoid lactones: a novel cannabinergic chemotype. *ACS Med Chem Lett*. 2014; 5:400–404. [PubMed: 24900848]
18. Nikas SP, Alapafuja SO, Papanastasiou I, Paronis CA, Shukla VG, Papahatjis DP, Bowman AL, Halikhedkar A, Han X, Makriyannis A. Novel 1',1'-chain substituted hexahydrocannabinols: 9beta-hydroxy-3-(1-hexyl-cyclobut-1-yl)-hexahydrocannabinol (AM2389) a highly potent cannabinoid receptor 1 (CB1) agonist. *J Med Chem*. 2010; 53:6996–7010. [PubMed: 20925434]
19. Mitsunobu O. The use of diethyl azodicarboxylate and triphenylphosphine in synthesis and transformation of natural products. *Synthesis*. 1981:1–28.
20. Papahatjis DP, Nahmias VR, Nikas SP, Andreou T, Alapafuja SO, Tsoinias A, Guo J, Fan P, Makriyannis A. C1'-Cycloalkyl side chain pharmacophore in tetrahydrocannabinols. *J Med Chem*. 2007; 50:4048–4060. [PubMed: 17672444]
21. Nikas SP, Thakur GA, Makriyannis A. Regiospecifically deuterated (–)-delta(9)-tetrahydrocannabivarin. *J Chem Soc, Perkin Trans*. 2002; 1:2544–2548.
22. White JM, Tunoori AR, Turunen BJ, Georg GI. [Bis(2-methoxyethyl)amino]sulfur trifluoride the Deoxo-Fluor reagent: application toward one-flask transformations of carboxylic acids to amides. *J Org Chem*. 2004; 69:2573–2576. [PubMed: 15049661]

23. Chaudhari SS, Akamanchi KG. Thionyl chloride–benzotriazole in methylene chloride: A convenient solution for conversion of alcohols and carboxylic acids expeditiously into alkyl chlorides and acid chlorides by simple titration. *Synlett*. 1999;1763–1765.
24. Shire D, Calandra B, RinaldiCarmona M, Oustric D, Pessegue B, BonninCabanne O, LeFur G, Caput D, Ferrara P. Molecular cloning, expression and function of the murine CB2 peripheral cannabinoid receptor. *Biochim Biophys Acta*. 1996; 1307:132–136. [PubMed: 8679694]
25. Khanolkar AD, Lu D, Ibrahim M, Duclos RI Jr, Thakur GA, Malan TP Jr, Porreca F, Veerappan V, Tian X, George C, Parrish DA, Papahatjis DP, Makriyannis A. Cannabilactones: a novel class of CB2 selective agonists with peripheral analgesic activity. *J Med Chem*. 2007; 50:6493–6500. [PubMed: 18038967]
26. Mukherjee S, Adams M, Whiteaker K, Daza A, Kage K, Cassar S, Meyer M, Yao BB. Species comparison and pharmacological characterization of rat and human CB2 cannabinoid receptors. *Eur J Pharmacol*. 2004; 505:1–9. [PubMed: 15556131]
27. Fukami T, Yokoi T. The emerging role of human esterases. *Drug Metab Pharmacokinet*. 2012; 27:466–477. [PubMed: 22813719]
28. Um PJ, Drueckhammer DG. Dynamic enzymatic resolution of thioesters. *J Am Chem Soc*. 1998; 120:5605–5610.
29. Durdagi S, Kapou A, Kourouli T, Andreou T, Nikas SP, Nahmias VR, Papahatjis DP, Papadopoulos MG, Mavromoustakos T. The application of 3D-QSAR studies for novel cannabinoid ligands substituted at the C1' position of the alkyl side chain on the structural requirements for binding to cannabinoid receptors CB1 and CB2. *J Med Chem*. 2007; 50:2875–2885. [PubMed: 17521177]
30. Nikas SP, Grzybowska J, Papahatjis DP, Charalambous A, Banijamali AR, Chari R, Fan P, Kourouli T, Lin S, Nitowski AJ, Marciniak G, Guo Y, Li X, Wang CL, Makriyannis A. The role of halogen substitution in classical cannabinoids: a CB1 pharmacophore model. *AAPS J*. 2004; 6:e30. [PubMed: 15760095]
31. Papahatjis DP, Nikas SP, Andreou T, Makriyannis A. Novel 1',1'-chain substituted delta(8)-tetrahydrocannabinols. *Bioorg Med Chem Lett*. 2002; 12:3583–3586. [PubMed: 12443781]
32. Papahatjis DP, Nikas SP, Kourouli T, Chari R, Xu W, Pertwee RG, Makriyannis A. Pharmacophoric requirements for the cannabinoid side chain. Probing the cannabinoid receptor subsite at C1'. *J Med Chem*. 2003; 46:3221–3229. [PubMed: 12852753]
33. Thakur GA, Nikas SP, Li C, Makriyannis A. Structural requirements for cannabinoid receptor probes. *Handb Exp Pharmacol*. 2005:209–246. [PubMed: 16596776]
34. Shih NY, Mangiaracina P, Green MJ, Ganguly AK. Synthesis of a carbocyclic analog of quercetin via a Barbier reaction. *Tetrahedron Lett*. 1989; 30:5563–5566.
35. Cheng Y, Prusoff WH. Relationship between the inhibition constant (K_i) and the concentration of inhibitor which causes 50% inhibition (I_{50}) of an enzymatic reaction. *Biochem Pharmacol*. 1973; 22:3099–3108. [PubMed: 4202581]
36. Wood JT, Smith DM, Janero DR, Zvonok AM, Makriyannis A. Therapeutic modulation of cannabinoid lipid signaling: metabolic profiling of a novel antinociceptive cannabinoid-2 receptor agonist. *Life Sci*. 2013; 92:482–491. [PubMed: 22749867]
37. Ballesteros, JA.; Weinstein, H. Integrated methods for the construction of three-dimensional models and computational probing of structure-function relations in G protein-coupled receptors. In: Stuart, CS., editor. *Methods in Neurosciences*. Vol. 25. Academic Press; San Diego: 1995. p. 366-428.
38. Chang G, Guida WC, Still WC. An internal-coordinate Monte Carlo method for searching conformational space. *J Am Chem Soc*. 1989; 111:4379–4386.
39. Saunders M, Houk KN, Wu YD, Still WC, Lipton M, Chang G, Guida WC. Conformations of cycloheptadecane—a comparison of methods for conformational searching. *J Am Chem Soc*. 1990; 112:1419–1427.
40. Kapur A, Hurst DP, Fleischer D, Whitnell R, Thakur GA, Makriyannis A, Reggio PH, Abood ME. Mutation studies of Ser7.39 and Ser2.60 in the human CB1 cannabinoid receptor: evidence for a serine-induced bend in CB1 transmembrane helix 7. *Mol Pharmacol*. 2007; 71:1512–1524. [PubMed: 17384224]

41. Palczewski K, Kumasaka T, Hori T, Behnke CA, Motoshima H, Fox BA, Le Trong I, Teller DC, Okada T, Stenkamp RE, Yamamoto M, Miyano M. Crystal structure of rhodopsin: A G protein-coupled receptor. *Science*. 2000; 289:739–745. [PubMed: 10926528]
42. Barnett-Norris J, Hurst DP, Buehner K, Ballesteros JA, Guarnieri F, Reggio PH. Agonist alkyl tail interaction with cannabinoid CB1 receptor V6.43/16.46 groove induces a helix 6 active conformation. *Int J Quantum Chem*. 2002; 88:76–86.
43. Barnett-Norris J, Hurst DP, Lynch DL, Guarnieri F, Makriyannis A, Reggio PH. Conformational memories and the endocannabinoid binding site at the cannabinoid CB1 receptor. *J Med Chem*. 2002; 45:3649–3659. [PubMed: 12166938]
44. Fiser A, Do RK, Sali A. Modeling of loops in protein structures. *Protein Sci*. 2000; 9:1753–1773. [PubMed: 11045621]
45. Sali A, Blundell TL. Comparative protein modelling by satisfaction of spatial restraints. *J Mol Biol*. 1993; 234:779–815. [PubMed: 8254673]
46. Ahn KH, Bertalovitz AC, Mierke DF, Kendall DA. Dual role of the second extracellular loop of the cannabinoid receptor 1: ligand binding and receptor localization. *Mol Pharmacol*. 2009; 76:833–842. [PubMed: 19643997]
47. Bertalovitz AC, Ahn KH, Kendall DA. Ligand binding sensitivity of the extracellular loop two of the cannabinoid receptor 1. *Drug Dev Res*. 2010; 71:404–411. [PubMed: 21170298]
48. Song ZH, Bonner TI. A lysine residue of the cannabinoid receptor is critical for receptor recognition by several agonists but not WIN55212-2. *Mol Pharmacol*. 1996; 49:891–896. [PubMed: 8622639]
49. Marcu J, Shore DM, Kapur A, Trznadel M, Makriyannis A, Reggio PH, Abood ME. Novel insights into CB1 cannabinoid receptor signaling: a key interaction identified between the extracellular-3 loop and transmembrane helix 2. *J Pharmacol Exp Ther*. 2013; 345:189–197. [PubMed: 23426954]
50. Paronis CA, Nikas SP, Shukla VG, Makriyannis A. Delta(9)-Tetrahydrocannabinol acts as a partial agonist/antagonist in mice. *Behav Pharmacol*. 2012; 23:802–805. [PubMed: 23075707]
51. Dixon DD, Sethumadhavan D, Benneche T, Banaag AR, Tius MA, Thakur GA, Bowman A, Wood JT, Makriyannis A. Heteroadamantyl cannabinoids. *J Med Chem*. 2010; 53:5656–5666. [PubMed: 20593789]

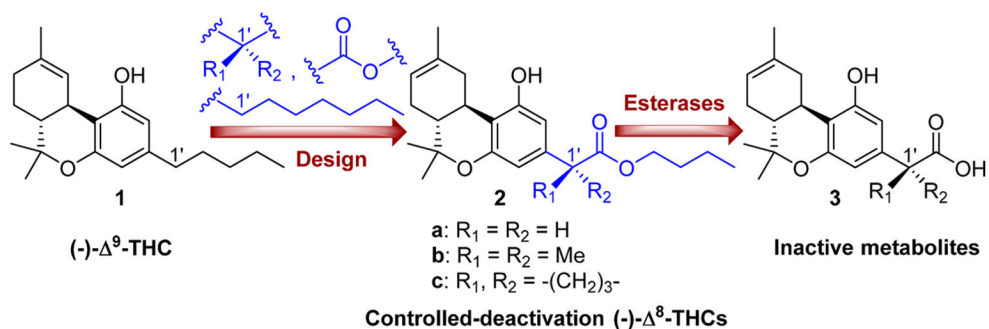


Figure 1. Design of the first-generation side chain carboxylated (-)- Δ^8 -tetrahydrocannabinols with controllable deactivation and structures of the prototype (-)- Δ^9 -THC and inactive metabolites.

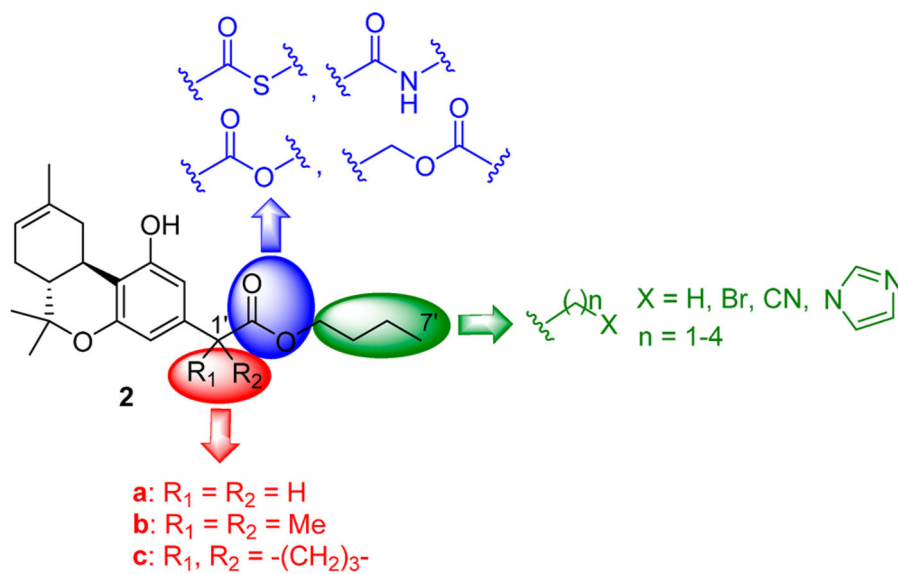


Figure 2. Structure–activity relationship summary of the metabolically vulnerable side chain pharmacophore in (-)-⁸-tetrahydrocannabinols.

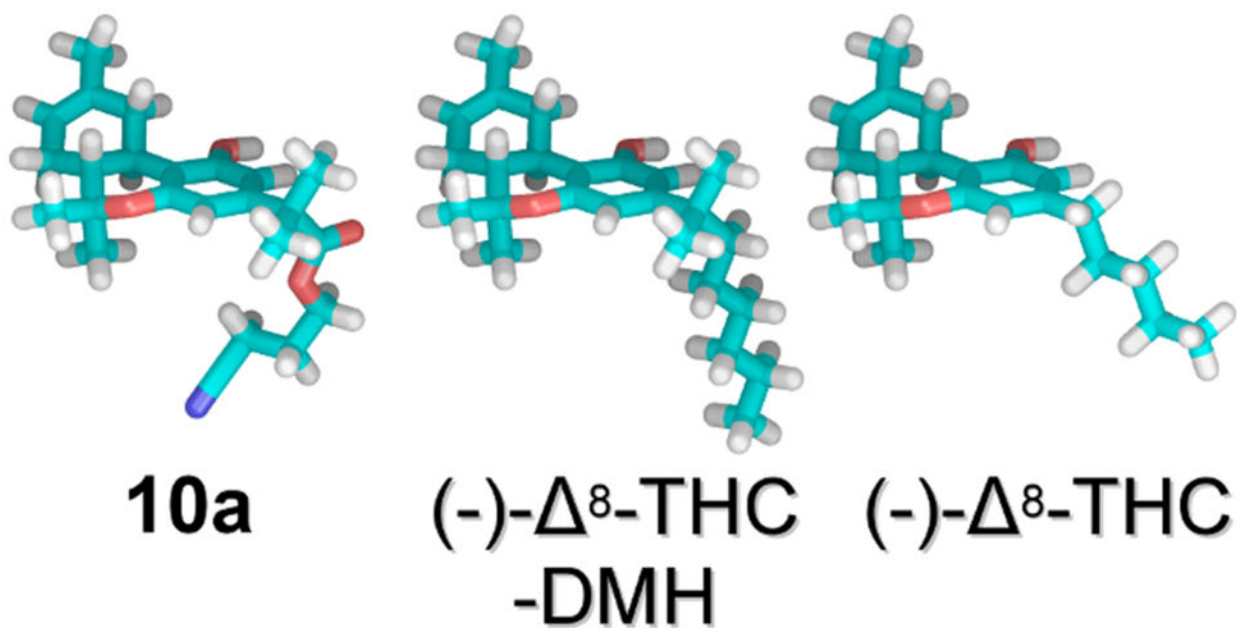


Figure 3.

10a is the lowest energy conformer that does not have the internal H-bond and is shown on the left. The (-)- Δ^8 -THC-DMH global minimum energy conformer is in the middle and (-)- Δ^8 -THC is on the right. All carbon atoms are shown in cyan.

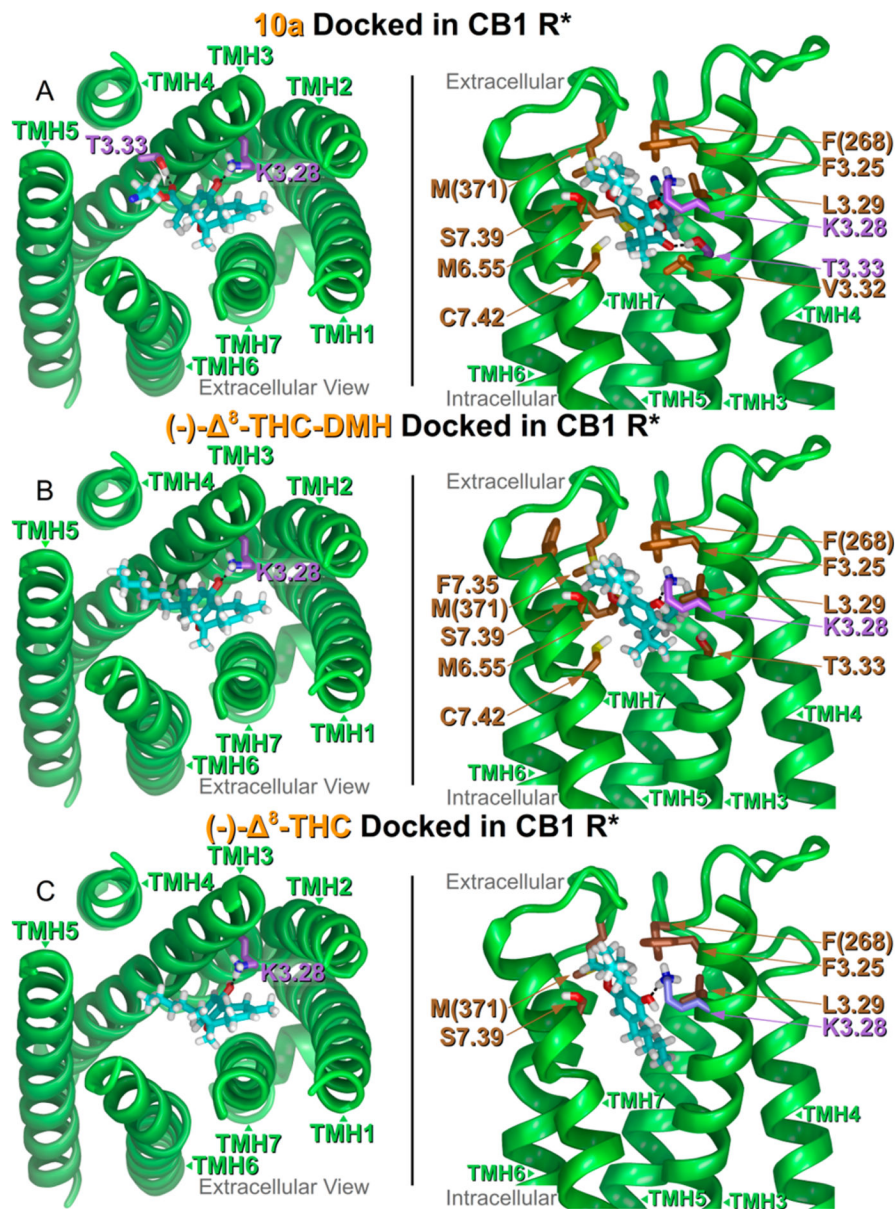


Figure 4. (A–C) (Left Panel, A–C) Extracellular viewpoint of each ligand/receptor complex. Termini and loops are not shown in this panel. Ligand carbons are colored cyan and hydrophilic interactions are displayed with amino acid carbons in violet. (Right Panel, A–C) Side view of ligand/receptor complexes as if looking through TMH1, 2 (not displayed). Hydrophobic interacting residues with better than -2.0 kcal/mol ligand interaction energies are displayed with brown carbons. Hydrophilic ligand interactions are displayed with the amino acid carbons in violet.

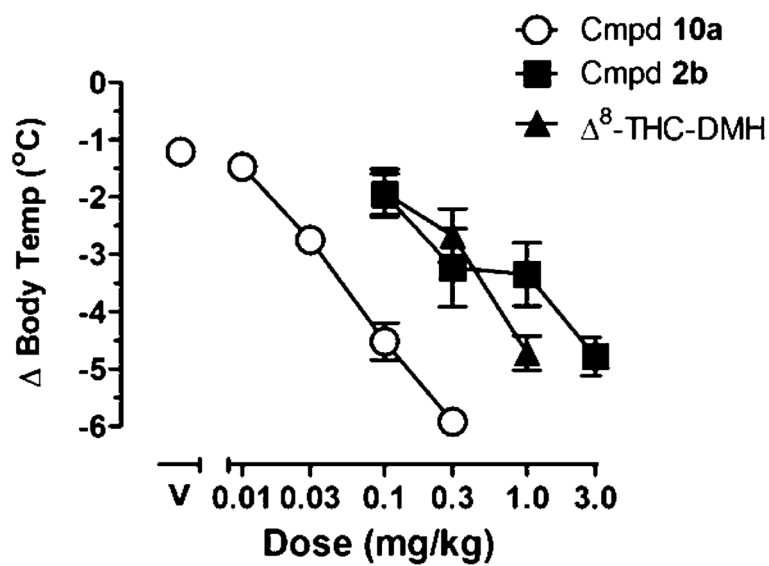


Figure 5. Effects of **10a**, **2b**, and Δ^8 -THC-DMH or vehicle (above V) on body temperature. Symbols represent the group mean \pm SEM ($n = 6$ rats). Abscissa, dose in mg/kg; ordinate, change in body temperature from an average baseline of 37.8 ± 0.1 °C. Data with compound **2b** and Δ^8 -THC-DMH published previously.¹⁶

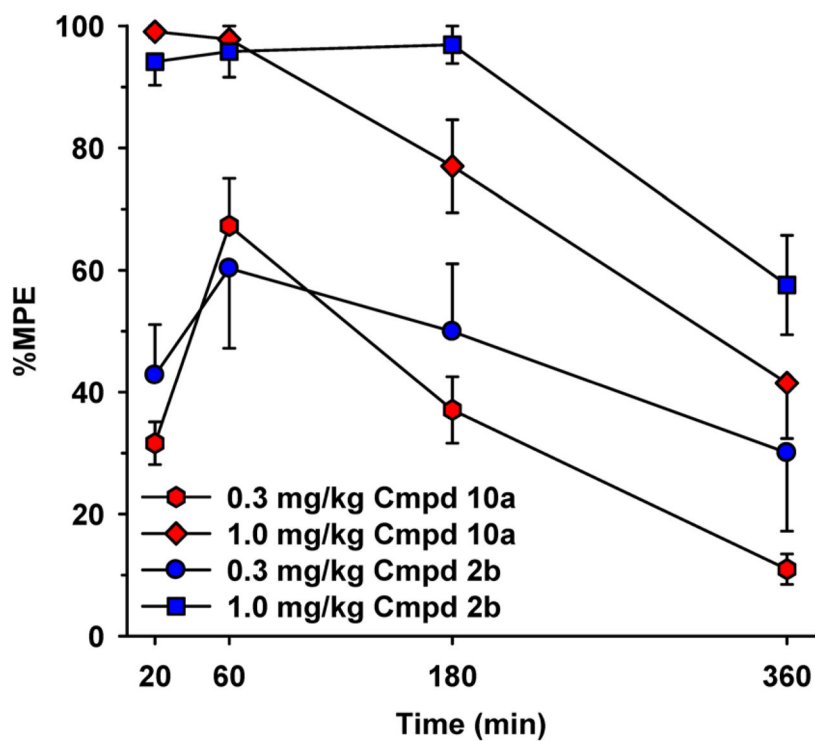
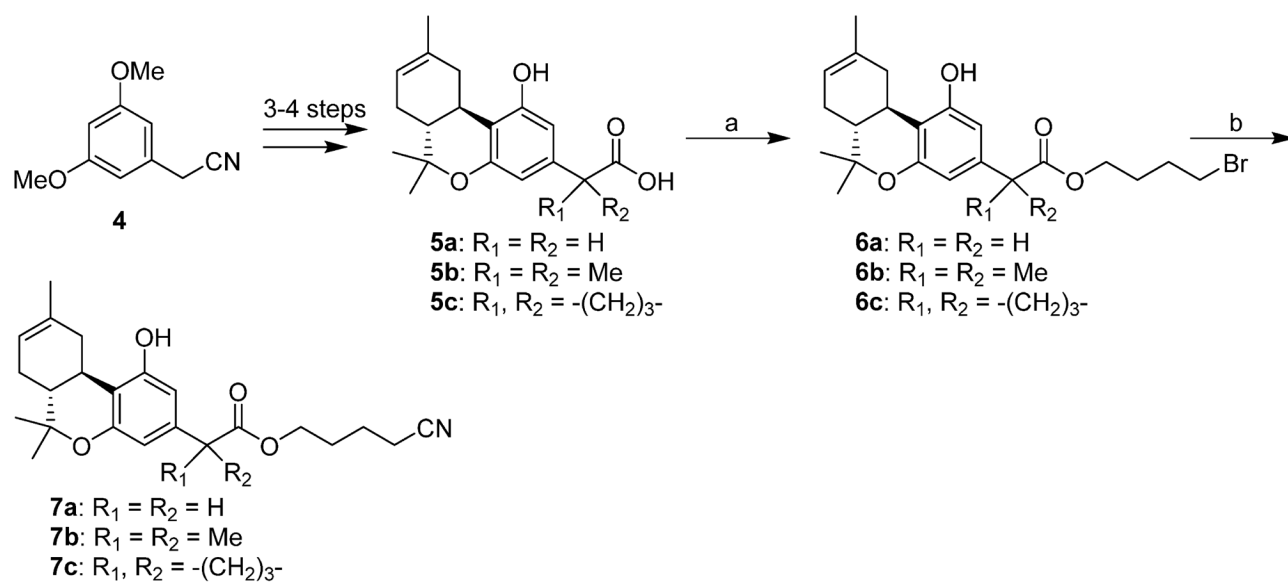
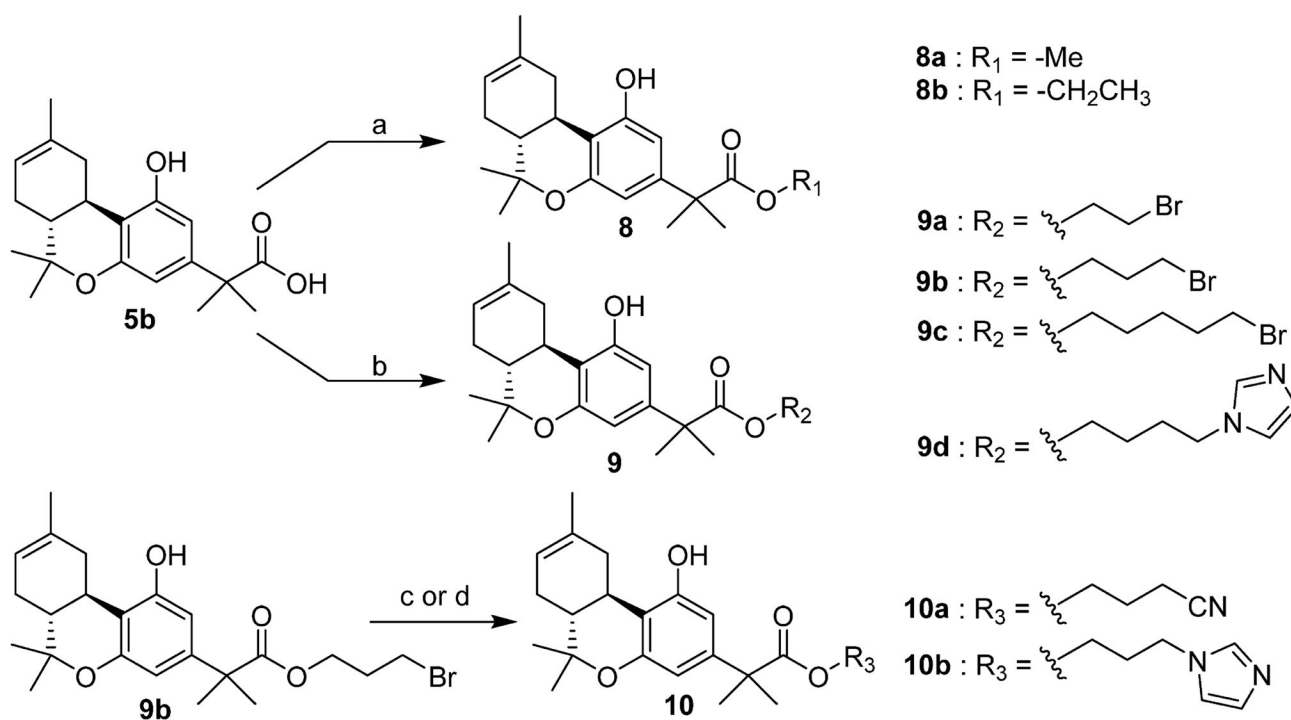


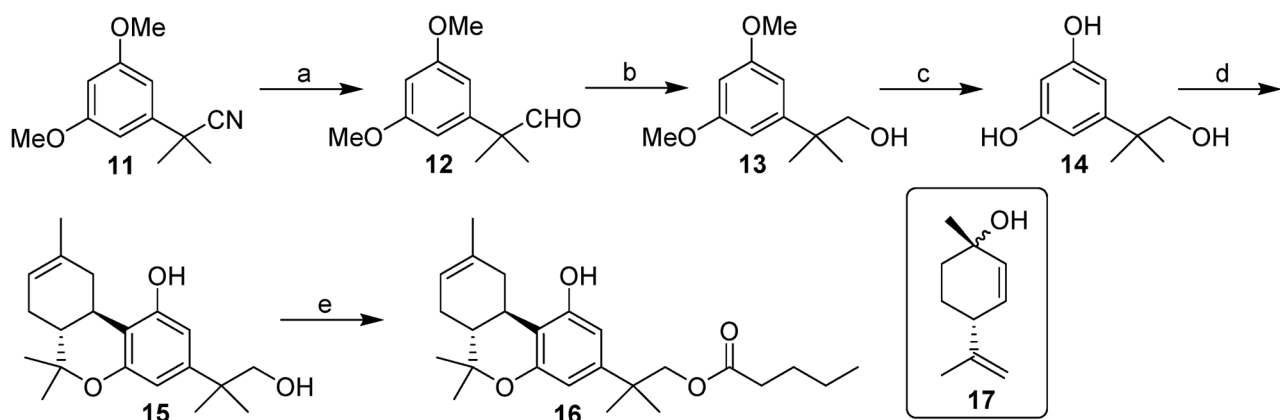
Figure 6. Tail-flick latencies in a hot water bath (52 °C) after administration of 0.3 and 1.0 mg/kg of compounds **10a** and **2b** at four time-points (20, 60, 180, and 360 min postadministration) using male CD-1 mice. Abscissa, time (min) after injection; ordinate, tail-flick withdrawal latencies expressed as a percentage of maximum possible effect (% MPE; group mean \pm SEM). Data for compound **2b** are reproduced from our earlier work.¹⁶

**Scheme 1^a**

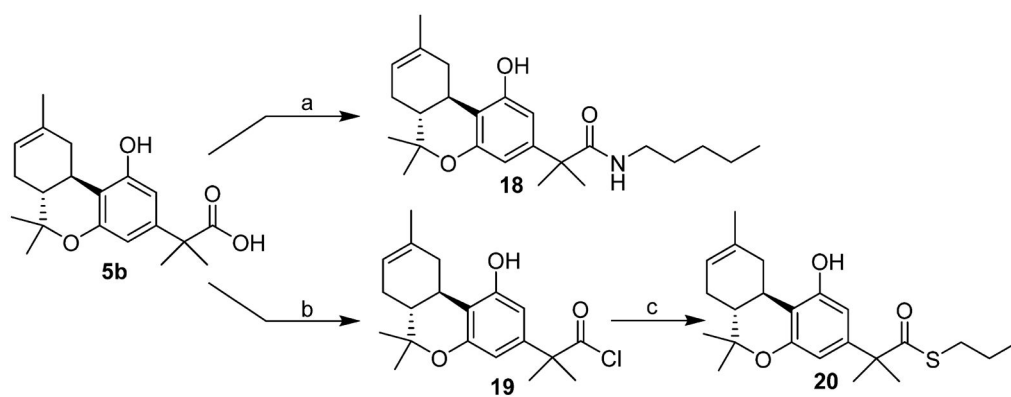
^aReagents and conditions: (a) $Br(CH_2)_4Br$, $NaHCO_3$, DMF, microwave irradiation, 165 °C, 12 min, 63% for **6a**, 53% for **6b**, and 45% for **6c**; (b) $NaCN$, DMSO, 50 °C, 12 h, 71% for **7a**, 54% for **7b**, and 63% for **7c**.

**Scheme 2^a**

^aReagents and conditions: (a) RI, NaHCO_3 , DMF, microwave irradiation, $165\text{ }^\circ\text{C}$, 12 min, 64% for **8a** and 87% for **8b**; (b) RBr, NaHCO_3 , DMF, microwave irradiation, $165\text{ }^\circ\text{C}$, 12 min, 48% for **9a**, 51% for **9b**, 47% for **9c**, and 47% for **9d**; (c) NaCN, DMSO, $50\text{ }^\circ\text{C}$, 12 h, 98% for **10a**; (d) imidazole, K_2CO_3 , DMSO, rt, 14 h, 41% for **10b**.

**Scheme 3^a**

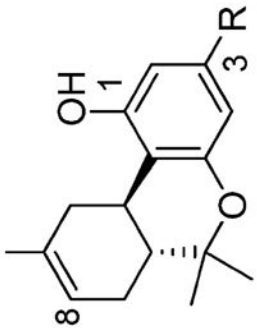
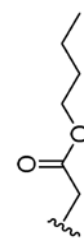
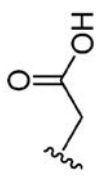
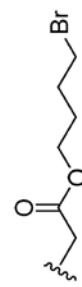

^aReagents and conditions: (a) DIBAL-H, CH₂Cl₂, -78 °C, 1 h, 92%, (b) NaBH₄, MeOH, rt, 1 h, 94%; (c) BBr₃, CH₂Cl₂, -78 °C, 15 min then rt, 1 h, 47%; (d) (+)-*cis/trans*-*p*-mentha-2,8-dien-1-ol (17), *p*-TSA, CHCl₃, microwave irradiation, 150 °C, 10 min, 28%; (e) DEAD, triphenylphosphine, CH₃(CH₂)₃COOH, THF, r, 20 h, 41%.

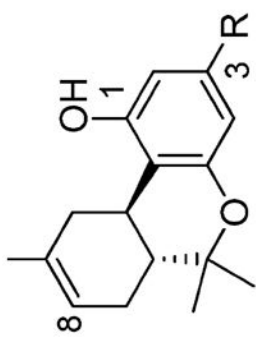
**Scheme 4^a**

^aReagents and conditions: (a) (MeOCH₂CH₂)₂NSF₃, Et₃N, CH₃(CH₂)₄NH₂, 0 °C, 15 min, then rt, 2 h, 70%; (b) SOCl₂, 1*H*-benzotriazole, CH₂Cl₂, rt, 20 min; (c) CH₃(CH₂)₂SH, pyridine, CH₂Cl₂, rt, 3 h, 23%, two steps.

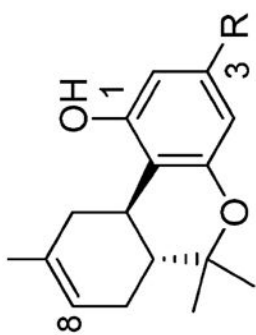
Table 1

Affinities (K_i) of Side Chain (-)-8-THC Analogues for CB1 and CB2 Cannabinoid Receptors ($\pm 95\%$ Confidence Limits) and Half-Lives ($t_{1/2}$) of Representative Compounds for Mouse Plasma Esterases

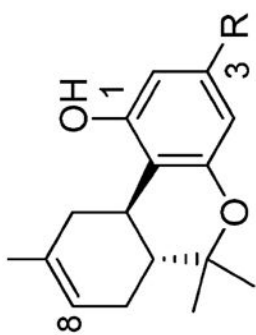
compd	R	$(K_i, \text{nm})^d$			mouse plasma $t_{1/2}$ (min) ^d
		rCB1	mCB2	bCB2	
(-)-8-THC		47.6 ^b	39.3 ^b	36.4 ^c	ND
2a		27.1 \pm 4.5	40.4 \pm 7.6	51.5 \pm 11.2	0.7
5a		>10,000	>10,000	ND	ND
6a		2.2 \pm 0.4	11.6 \pm 3.7	7.1 \pm 2.2	1.7
7a		14.3 \pm 3.2	2.1 \pm 0.3	1.2 \pm 0.4	3.2



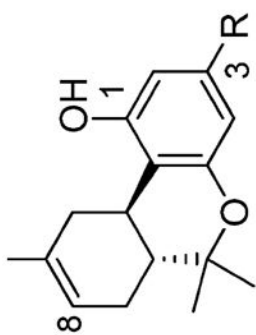
compd	R	(K _i , nm ²) ^d			mouse plasma t _{1/2} (min) ^d
		rCB1	mCB2	bCB2	
2b		0.3 ± 0.1	2.1 ± 1.1	1.7 ± 0.4	12.4
5b		>10,000	>10,000	ND	ND
8a		83.1 ± 7.3	36.9 ± 5.8	34.5 ± 7.4	ND
8b		2.7 ± 0.7	0.5 ± 0.3	1.5 ± 0.2	ND
16		0.5 ± 0.1	1.2 ± 0.3	1.0 ± 0.4	9.5



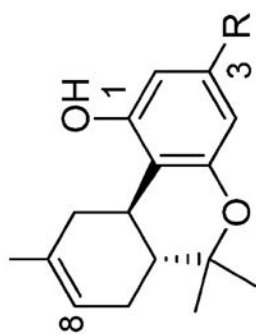
compd	R	(K _i , nm ²) ^d			mouse plasma t _{1/2} (min) ^d
		rCB1	mCB2	bCB2	
15		447 ± 85	>10,000	>10,000	ND
9a		7.7 ± 1.3	3.2 ± 1.2	2.9 ± 0.9	ND
9b		0.8 ± 0.3	1.1 ± 0.3	0.7 ± 0.2	ND
6b		1.2 ± 0.4	0.9 ± 0.3	0.8 ± 0.3	12.9
9c		1.2 ± 0.5	1.1 ± 0.03	0.6 ± 0.1	ND



compd	R	(K _i , nm) ^d			mouse plasma t _{1/2} (min) ^d
		rCB1	mCB2	bCB2	
10a		0.5 ± 0.2	0.8 ± 0.3	1.4 ± 0.7	46.5
10b		3.4 ± 1.1	2.1 ± 0.5	1.3 ± 0.3	271
7b		0.7 ± 0.07	0.1 ± 0.2	0.9 ± 0.3	40.4
9d		29.1 ± 4.1	8.2 ± 2.3	7.7 ± 1.1	392
18		6.3 ± 2.2	9.2 ± 2.1	2.8 ± 0.5	Stable ^e



compd	R	(K _i , nM) ^d			mouse plasma t _{1/2} (min) ^d
		rCB1	mCB2	bCB2	
20		0.5 ± 0.1	0.8 ± 0.3	0.7 ± 0.1	312
2c	; 	0.7 ± 0.2	3.0 ± 0.5	3.0 ± 0.7	36.3
5c	; 	>10,000	>10,000	ND	ND
6c	; 	0.3 ± 0.1	3.7 ± 0.7	0.7 ± 0.3	47.9



compd	R	$(K_i, \text{nm})^a$		mouse plasma $t_{1/2}$ (min) ^d	
		rCB1	mCB2		bCB2
7c		0.9 ± 0.3	1.5 ± 0.5	1.8 ± 0.3	115

^a Affinities for CB1 and CB2 were determined using rat brain (CB1) or membranes from HEK293 cells expressing mouse or human CB2 and [³H]CP-55,940 as the radioligand following previously described procedures.^{18,20,51} Data were analyzed using nonlinear regression analysis. K_i values were obtained from three independent experiments performed in triplicate and are expressed as the mean of the three values.

^b Reported previously.³³

^c Reported previously.¹⁴

^d Half-lives ($t_{1/2}$) for mouse plasma were determined as described under Experimental Section.

^e No observable hydrolysis within 5 h.

ND: not determined.

Table 2Functional Potencies (EC₅₀) of Selected (-)-⁸-THC Ester Analogues for the rCB1 Cannabinoid Receptor

compd	rCB1 (EC ₅₀ , nM) ^a		<i>E</i> _(max) (%) ^d
	3-points ^b	8-points ^c	
7a	10–100		
2b	<1	0.5 (0.1–1.2) ^e	92 ^e
8b	1–10		
10a	<1	0.9 (0.3–1.5)	89
10b	1–10		
7b	1–10		
18	1–10		
2c	<1	0.4 (0.2–1.2) ^e	90 ^e
7c	1–10		

^aFunctional potencies at rCB1 receptor were determined by measuring the decrease in forskolin-stimulated cAMP levels, as described in Experimental Section. 16,18

^bThree point data were obtained from one experiment (3 points) run in duplicate (less accurate EC₅₀ values).

^cData are average of two independent experiments (8 points) run in triplicate, and 95% confidence intervals for the EC₅₀ values are given in parentheses. EC₅₀ values were calculated using nonlinear regression analysis.

^dForskolin stimulated cAMP levels were normalized to 100% and *E*_(max) is the maximum inhibition of forskolin stimulated cAMP levels and is presented as the percentage of CP-55,940 response at 500 nM.

^eReported previously.¹⁶

Table 3

Comparison of Side Chain Dihedral Values for Global Minimum Energy Conformers and Binding Affinities (K_i) of Key Analogues

side chain dihedral	$K_i = 0.5 \text{ nM (rCB1), } = 0.8 \text{ nM (mCB2)}$ (deg)		$K_i = 0.9 \text{ nM (rCB1), } = 1.4 \text{ nM}$ (mCB2) (deg)	$K_i = 47.6 \text{ nM (rCB1), } =$ 39.3 nM (mCB2) (deg)
	10a	no int H-bond 10a	(-)- ⁸ -THC-DMH	(-)- ⁸ -THC
C2-C3-C1'-C2'	-38.3	-54.5	-52.3	-85.6
C3-C1'-C2'-(C3', O3')	-60.2	-68.7	-60.0	179.9
C1'-C2'-(C3', O3')-C4'	174.6	176.1	175.2	-179.9
C2'-(C3', O3')-C4'-C5'	-164.7	-174.5	179.5	180.0
(C3', O3')-C4'-C5'-C6'	54.4	61.4	179.1	
C4'-C5'-C6'-C7'	54.3	179.1	180.0	

Table 4

Calculated log *P* and tPSA Values for (-)-⁸-THC-DMH, 2b, and 10a, and Duration of Their Hypothermic Effects in Rats

compd	clogP ^a	tPSA ^a	duration of hypothermic effects in rats ^b
(-)- ⁸ -THC-DMH	9.1	29.5	<i>t</i> > 12 h
2b	6.6	55.8	<i>t</i> = 6–12 h
10a	5.0	79.5	<i>t</i> < 6 h

^aCalculations were performed using ChemBioDraw Ultra 14.0 software.

^bHypothermic effects were determined using equiactive doses of the test compounds.